

MIT Open Access Articles

*Synthesis and Reversible Reductive Coupling of
Cationic, Dinitrogen-Derived Diazoalkane Complexes*

The MIT Faculty has made this article openly available. *Please share*
how this access benefits you. Your story matters.

Citation: Curley, John J., Tetsuro Murahashi, and Christopher C. Cummins. "Synthesis and Reversible Reductive Coupling of Cationic, Dinitrogen-Derived Diazoalkane Complexes." *Inorganic Chemistry* 48.15 (2009) : 7181-7193. Copyright © 2009 American Chemical Society

As Published: <http://dx.doi.org/10.1021/ic900495s>

Publisher: American Chemical Society

Persistent URL: <http://hdl.handle.net/1721.1/64725>

Version: Author's final manuscript: final author's manuscript post peer review, without publisher's formatting or copy editing

Terms of Use: Article is made available in accordance with the publisher's policy and may be subject to US copyright law. Please refer to the publisher's site for terms of use.



Synthesis and Reversible Reductive Coupling of Cationic, Dinitrogen-Derived Diazoalkane Complexes

John J. Curley, Tetsuro Murahashi,[†] and Christopher C. Cummins*

Department of Chemistry, Massachusetts Institute of Technology, 77 Massachusetts Avenue, Room 6-435, Cambridge, Massachusetts 02139

A series of cationic diazoalkane complexes $[4\text{-RC}_6\text{H}_4\text{C(H)NNMo(N[}t\text{-Bu]Ar)}_3][\text{AlCl}_4]$, $[\mathbf{1}\text{-R}][\text{AlCl}_4]$ ($\text{R} = \text{NMe}_2, \text{Me}, \text{H}, \text{Br}, \text{CN}, \text{Ar} = 3,5\text{-C}_6\text{H}_3\text{Me}_2$) have been prepared by treatment of the N_2 -derived diazenido complex $\text{Me}_3\text{SiNNMo(N[}t\text{-Bu]Ar)}_3$ with $4\text{-RC}_6\text{H}_4\text{CHO}$ and 2 equiv AlCl_3 . The structures of $[\mathbf{1}\text{-H}][\text{AlCl}_4]$ and $[\mathbf{1}\text{-NMe}_2][\text{AlCl}_4]$ were determined by X-ray crystallography. The C–N and N–N stretching modes were identified by a combined IR and Raman spectroscopy study, and other physical properties are discussed in detail. The electrochemical reduction potential for $[\mathbf{1}\text{-R}][\text{AlCl}_4]$ was shown to be linear with the Hammett σ parameter. This reduction process forms the C–C bonded dimer, $\mu\text{-(4-RC}_6\text{H}_4\text{C(H)NN)}_2[\text{Mo(N[}t\text{-Bu]Ar)}_3]_2$ that was characterized by X-ray crystallography for $\text{R} = \text{H}$. Possible mechanisms for the formation of this dimer are presented. Both electrochemical investigations and quantum chemical calculations are used to describe the odd-electron complex $4\text{-RC}_6\text{H}_4\text{C(H)NNMo(N[}t\text{-Bu]Ar)}_3$, $\mathbf{1}\text{-R}$, that is an intermediate in formation of $[\mathbf{1}\text{-R}]_2$. The C–C bond in $[\mathbf{1}\text{-R}]_2$ is redox non-innocent and is broken upon oxidation. This reaction was used to prepare $[\mathbf{1}\text{-H}][\text{A}]$ ($\text{A} = \text{PF}_6^-, \text{OTf}^-$), and possible uses of this property in charge-storage devices are discussed.

Introduction

A great deal of energy has been expended optimizing methods for the chemical fixation of dinitrogen.^{1–7} Of these methods, the Haber-Bosch process, that forms NH_3 from N_2 and H_2 , is the most well-studied and currently the most widespread process for nitrogen fixation.⁸ Ammonia produced by this process may be incorporated into organic molecules in a subsequent synthetic step. However, a more synthetically efficient route to nitrogen-containing organic molecules would directly incorporate N_2 into organic fragments without the intermediacy of ammonia.^{9–18} Such a synthetic protocol could be designed to avoid the need for H_2 , which currently is formed by steam reforming of CH_4 producing the greenhouse gas CO_2 . Therefore, the development of new chemical methods to incorporate nitrogen atoms into organic molecules without the need for reduction of N_2 to ammonia would effect both a more efficient and environmentally benign production of nitrogen-containing organic molecules. For these reasons, this area of research is under active exploration.^{11–19}

In order to bypass traditional schemes for nitrogen fixation, it is important that the product of N_2 transfer be a useful synthetic precursor for organic reactions. One class of compounds that meets this criteria is that of the diazoalkanes, which are important precursors to nitrogen-containing organic molecules. These molecules react by 1,3-dipolar addition reactions to incorporate

both nitrogen atoms into organic functional groups.^{20–22} Thereby, diazoalkanes are used as synthons for pyrazolines,^{23–27} compounds used in asymmetric ligand²⁵ and drug design.^{28,29}

Diazoalkane complexes may be made from coordinated N_2 , such as one N_2 ligand in $(\text{N}_2)_2\text{M(diphos)}_2$ ($\text{M} = \text{Mo}, \text{W}$; diphos = chelating diphosphine),^{1,17,20,30–32} or by treatment of a transition-metal fragments with an organic diazoalkane to form a coordination complex.^{33–40} For instance, photolysis of gem-dibromides (i.e., Me_2CBr_2) in the presence of $(\text{N}_2)_2\text{W(diphos)}_2$ has been shown to afford $[\text{Me}_2\text{CNNW(diphos)}_2\text{Br}]^+$.³¹ An alternative route to diazoalkane complexes of this type has been accomplished by the sequential treatment of $(\text{N}_2)_2\text{M(diphos)}_2$ with a strong acid followed by an aldehyde. In those diazoalkane complexes that are prepared by addition of an organic diazoalkane to a transition-metal complex, either hydrazones or diazenes may serve as precursors to the diazoalkane ligand.^{41,42} In many cases, compounds arrived at by either synthetic route are stable with regard to N_2 loss that would lead to formation of a carbene complex.^{1,20,33,43–46} However, diazoalkanes also remain synthons of choice to generate metal carbenes.^{33–37,44–52}

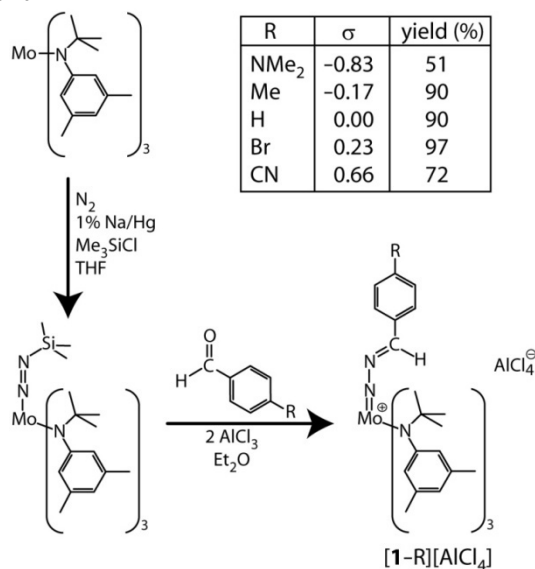
Given that diazoalkane complexes may be made by addition of a diazoalkane to a coordinatively unsaturated transition metal complex, one might expect that Ph_2CN_2 would add to $\text{Mo(N[}t\text{-Bu]Ar)}_3$ to form a diazoalkane complex, in analogy to the odd-electron compound $\text{PhCNMo(N[}t\text{-Bu]Ar)}_3$ ($\text{Ar} = 3,5\text{-C}_6\text{H}_3\text{Me}_2$).^{53–}

⁵⁵ However, we found that both Ph₂CN₂ and N₂O engage in facile reactions with Mo(N[*t*-Bu]Ar)₃ that form NMo(N[*t*-Bu]Ar)₃.^{56,57} As a result, odd-electron diazoalkane complexes cannot be prepared by simple coordination of a free diazoalkane to Mo(N[*t*-Bu]Ar)₃. This finding motivated us to develop alternative routes for the synthesis of the complexed diazoalkane functional group in order to prepare complexes of the formula 4-RC₆H₄C(H)NNMo(N[*t*-Bu]Ar)₃, **1-R** (R = NMe₂, Me, H, Br, CN). The N₂-derived diazenido compound, Me₃SiNNMo(N[*t*-Bu]Ar)₃ is formed in high yields by treatment of Mo(N[*t*-Bu]Ar)₃ with a mixture of 1% Na/Hg and Me₃SiCl under an atmosphere of N₂.⁵⁸ We thought that the terminal nitrogen of the trimethylsilyl diazenido would be sufficiently nucleophilic to participate in reactions that form N–C bonds, and therefore, protocols were developed to convert this diazenido fragment into a coordinated diazoalkane.

Results and Discussion

Synthesis and Structure of Diazoalkane Complexes. Inspired by organic condensation reactions between aldehydes and amines,⁵⁹ we explored treatment of Me₃SiNNMo(N[*t*-Bu]Ar)₃ with aldehydes. A related strategy has been successful in the case of [H₂NNM(diphos)₂F][BF₄] (M = Mo, W), which undergoes reactions with ketones to lose 1 equiv of H₂O forming [R₂CNNM(diphos)₂F][BF₄].^{17,30,32} Because Brønsted acids are incompatible with our ancillary ligands, strong Lewis acids were used in place of protic conditions. Accordingly, Me₃SiNNMo(N[*t*-Bu]Ar)₃ was treated with 1 equiv of AlCl₃ and PhCHO in Et₂O, upon which the product diazoalkane complex [PhC(H)NNMo(N[*t*-Bu]Ar)₃][AlCl₄], **[1-H][AlCl₄]**, precipitates from the reaction mixture as a red powder (Scheme 1). However, half of the starting diazenido complex was recovered from the reaction mixture when this procedure was followed. When 2 equiv of AlCl₃ were used, **[1-H][AlCl₄]** was isolated from the reaction mixture in 90% yield by filtration. We presume that the soluble byproduct of this synthesis

Scheme 1^a



^a Synthesis of diazoalkane complexes. Yields and Hammett σ parameters for the aryl substituent are given in the Scheme.

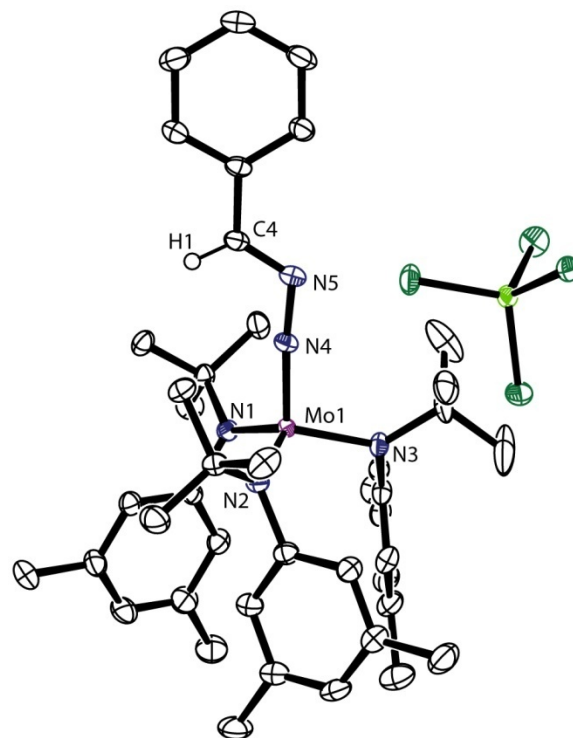


Figure 1. An ORTEP drawing of **[1-H][AlCl₄]** with 50% probability ellipsoids. Hydrogen atoms having calculated atomic positions are omitted for clarity. Selected bond lengths and angles are given in the text.

is $[\mu-(\text{Me}_3\text{SiO})\text{AlCl}_2]_2$.^{60,61} The salt, **[1-H][AlCl₄]**, is stable with regard to N₂ loss. In fact, **[1-H][AlCl₄]** may be heated to 60 °C in CDCl₃ for several days without noticeable decomposition (as assayed by ¹H NMR), and solids may be repeatedly melted at 192 °C.

Employing N₂ as the synthon for the diazoalkane ligand of **[1-H][AlCl₄]** made it convenient to isotopically label the diazoalkane fragment via use of ¹⁵N₂. The ¹⁵N NMR spectrum of ¹⁵N₂-**[1-H][AlCl₄]** depicts two doublets of doublets centered at 384 and 417 ppm. These values agree well with the chemical shifts of 397 and 422 ppm obtained from DFT calculations (Table S1). The deshielding of these nitrogen nuclei has been attributed to low-energy $n_{\text{N}} \rightarrow \pi^*$ circulations.⁶² The observed ¹J_{NN} = 17 Hz coupling is consistent with literature data for metal diazenido compounds in which the metal-N-N angle is approximately linear.⁶² We assign the more downfield signal as the nitrogen bound to Mo based upon both proton coupling and comparison to related compounds such as Me₃SiNNMo(N[*t*-Bu]Ar)₃. The proton-coupled ¹⁵N NMR spectrum revealed N–H couplings of ³J_{NH} = 6 Hz and ²J_{NH} = 3 Hz consistent with the expectation that the magnitude of the ²J_{NH} coupling through an *sp*² hybridized atom will be smaller than that of the ³J_{NH} coupling for a planar diazoalkane ligand.⁶³

The synthesis of **[1-H][AlCl₄]** requires both that an oxygen atom be removed from the aldehyde, breaking the C=O double bond, and that a C=N double bond be formed during the reaction. It is also a redox reaction in which molybdenum goes from the +4 to the +6 formal oxidation state. We found it interesting that such a transformation gave a diazoalkane-containing product in high yields. Moreover, the thermal stability of **[1-H][AlCl₄]** contrasts

with previous use of this diazoalkane, PhC(H)N_2 , to study carbene transfer reactions which occur via N_2 loss.^{35,41} Therefore, we sought to expand the synthetic methodology in a manner suitable for systematic comparison of the properties of such diazoalkane complexes.⁴¹ For this purpose, we chose to vary the substituent in the 4-position of the diazoalkane aryl ring. This strategy allows us to draw upon linear free energy relationships established within the field of physical organic chemistry as a guide for comparison.^{35,64,65} We found that with only minor modifications in the protocol, the synthesis of $[\mathbf{1-H}][\text{AlCl}_4]$ could be successfully applied for the synthesis of four other diazoalkane complexes $[\mathbf{4-R}]\text{C}_6\text{H}_4\text{C(H)NNMo}(\text{N}[\textit{t}\text{-Bu}]\text{Ar})_3][\text{AlCl}_4]$, $[\mathbf{1-R}][\text{AlCl}_4]$ ($\text{R} = \text{NMe}_2$, 51%; Me, 90%; Br, 97%; CN, 72% isolated yield; Scheme 1) by combination of the appropriate aldehyde, AlCl_3 , and $\text{Me}_3\text{SiNNMo}(\text{N}[\textit{t}\text{-Bu}]\text{Ar})_3$.

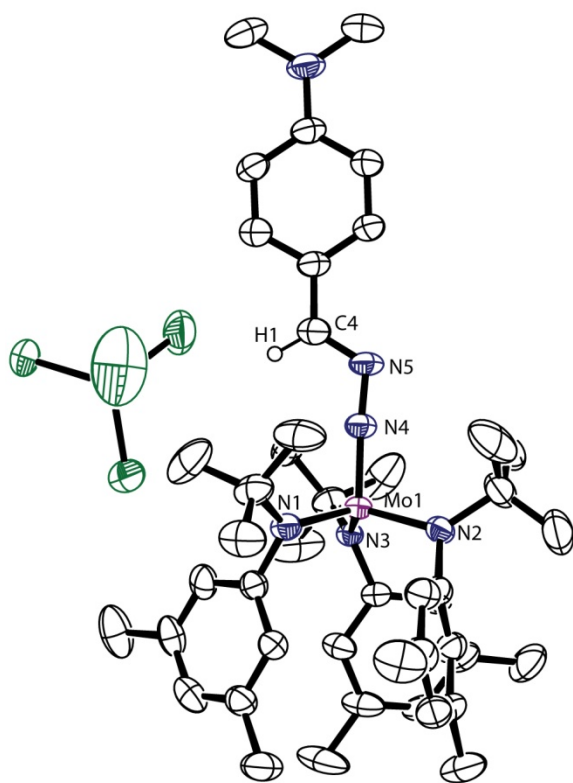


Figure 2. An ORTEP drawing of $[\mathbf{1-NMe}_2][\text{AlCl}_4]$ with 50% probability ellipsoids. Hydrogen atoms having calculated atomic positions are omitted for clarity. Selected bond lengths and angles are given in the text.

Crystals of $[\mathbf{1-H}][\text{AlCl}_4]$ suitable for X-ray diffraction were grown from THF/*n*-pentane at -35°C . The X-ray crystal structure of $[\mathbf{1-H}][\text{AlCl}_4]$ shows that the three anilide ligands are oriented in the same direction, imparting a *pseudo*- C_3 symmetry to the lower hemisphere of the molecule that is broken by the C_s symmetric diazoalkane ligand (Figure 1). The Mo–N4 distance of 1.7326(18) Å suggests π bonding between Mo and the diazoalkane N. The N4–N5 distance of 1.336(2) Å and N5–C4 distance of 1.290(3) Å are consistent with the description that the diazoalkane ligand is reduced by backbonding from Mo. Accordingly, the N–N distance is substantially longer than what one would expect for a free

diazoalkane (*cf.* 1.13(4) Å for H_2CN_2).^{66,67} A slightly different set of internuclear distances were found in the single-crystal X-ray structure of $[\mathbf{1-NMe}_2][\text{AlCl}_4]$: Mo–N4, 1.730(2) Å; N4–N5, 1.317(3) Å; and N5–C4, 1.312(4) Å (Figure 2). The NMe_2 group is coplanar with the aryl ring, maximizing the electron donation of this substituent into the π network of the diazoalkane. Presumably, this electronic perturbation is responsible for the small alteration in internuclear distances in $[\mathbf{1-NMe}_2][\text{AlCl}_4]$ compared to $[\mathbf{1-H}][\text{AlCl}_4]$. Both sets of metrics compare well with those obtained for other terminally bound, singly-bent diazoalkanes coordinated to Mo and W.^{17,68–72} Diazoalkane ligands are described as singly-bent when the C–N–N angle is approximately 120° and the metal–N–N angle is close to 180° ,³³ as is the case for the compounds reported here. The N4–N5–C4 and Mo1–N4–N5 angles are $117.86(19)^\circ$ and $174.21(16)^\circ$ in $[\mathbf{1-H}][\text{AlCl}_4]$ and $116.9(3)^\circ$ and $176.0(2)^\circ$ in $[\mathbf{1-NMe}_2][\text{AlCl}_4]$.

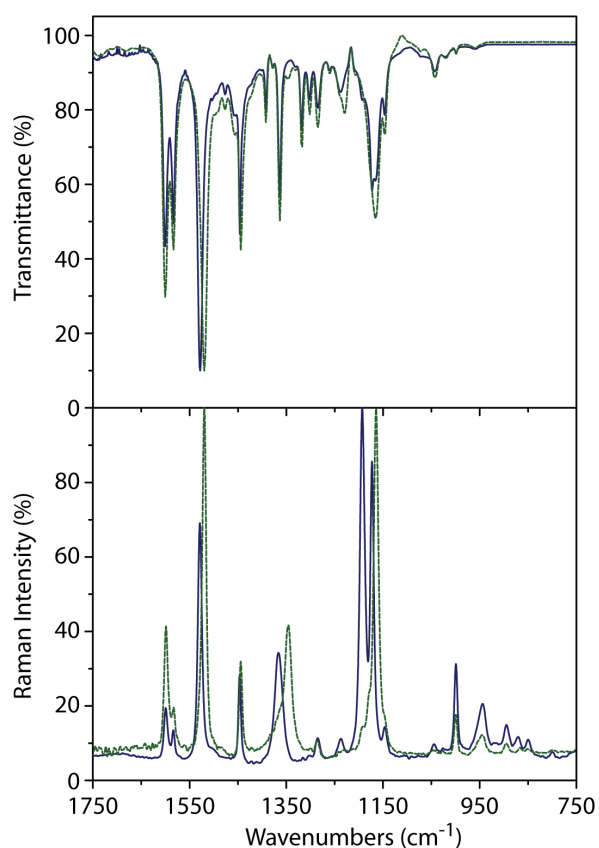


Figure 3. IR (above) and Raman (below) spectra of $[\mathbf{1-H}][\text{AlCl}_4]$ (solid blue line) and $^{15}\text{N}_2$ - $[\mathbf{1-H}][\text{AlCl}_4]$ (dashed green line) in CDCl_3 at 20°C .

Electronic and Vibrational Spectroscopy. Diazoalkane complexes typically have characteristic stretching modes that are suitable for study by vibrational spectroscopy.^{20,33} To gain information about the vibrational structure of the coordinated diazoalkane ligand, infrared and Raman spectroscopy data were collected for complexes $[\mathbf{1-R}][\text{AlCl}_4]$ ($\text{R} = \text{NMe}_2$, Me, H, Br, CN). Due to the low symmetry of the five cations (approximately C_s) most vibrational modes of the diazoalkane ligand give rise to bands in both the Raman and IR spectrum (Figures S15–S20). The Raman

spectrum of $[\mathbf{1-H}][\text{AlCl}_4]$ contains five intense bands that are attributed to vibrational modes of the PhC(H)N_2 ligand located at 1528, 1446, 1366, 1193, and 1173 cm^{-1} . The band located at 1528 cm^{-1} in both the IR and Raman spectra is in the spectral region for which the predominantly C=N stretching mode of the η^1 -diazalkane ligand is expected.^{20,33} This assignment was supported by a $^{15}\text{N}_2$ -labeling experiment in which the corresponding band for $^{15}\text{N}_2$ - $[\mathbf{1-H}][\text{AlCl}_4]$ was found at 1520 cm^{-1} (Figure 3). The 8 cm^{-1} shift of the C=N stretching mode is smaller than would be predicted by a harmonic oscillator model (24 cm^{-1}), indicating that this vibrational mode couples to others. Coupling of the C=N and N=N vibrational modes is observed for both coordinated and free diazoalkanes.^{73,74} Additionally, for aryl diazenido complexes it has been demonstrated that the aryl C-H modes couple into the N=N oscillator.^{75,76}

Numeric frequency calculations carried out on the model complex $[\text{PhC(H)NNMo}(\text{NH}_2)_3]^+$, $[\mathbf{1-m}]^+$, support the assignment of the band at 1528 cm^{-1} as a primarily C=N oscillator (Table S3). These computational results predicted a vibration 1459 cm^{-1} due to a C-H wagging motion of hydrogen atoms bound to the Ph group. Accordingly, a band for $[\mathbf{1-H}][\text{AlCl}_4]$ was found at 1446 cm^{-1} . Moreover, this band shifts just 2 cm^{-1} upon substitution of $^{15}\text{N}_2$ for $^{14}\text{N}_2$, consistent with nature of the described vibrational mode.

Table 1. Vibrational data for the diazoalkane ligand in cm^{-1} .

Complex	ν_1	ν_2	ν_3
$[\mathbf{1-NMe}_2][\text{AlCl}_4]$	1498	— ^a	— ^a
$[\mathbf{1-Me}][\text{AlCl}_4]$	1526	1367	1197
$[\mathbf{1-H}][\text{AlCl}_4]$	1528	1366	1193
$^{15}\text{N}_2$ - $[\mathbf{1-H}][\text{AlCl}_4]$	1520	1346	1164
$[\mathbf{1-Br}][\text{AlCl}_4]$	1525	1367	1192
$[\mathbf{1-CN}][\text{AlCl}_4]$	1524	1361	1193

^a Sample fluorescence prevented the acquisition of Raman data.

A band that is only intense in the Raman spectrum of $[\mathbf{1-H}][\text{AlCl}_4]$ was located at 1366 cm^{-1} . The Raman activity of this band suggested to us that it is largely composed of N=N stretching character which is expected to give rise to a smaller change in dipole moment than the C=N stretching motion. When $^{15}\text{N}_2$ is incorporated into the diazoalkane ligand this band shifts to 1346 cm^{-1} . The 20 cm^{-1} shift that occurs upon isotopic substitution is twice as large as the shift found for the predominantly C=N stretching mode, but is less than half the predicted value of 46 cm^{-1} for a harmonic N=N oscillator. Calculations carried out on $[\mathbf{1-m}]^+$ found a band at 1363 cm^{-1} that is described by a mixture of both the C=N and N=N stretching modes combined with a wagging of the hydrogen atom attached to the diazoalkane carbon. For this reason, the band at 1366 cm^{-1} is attributed to a highly coupled vibrational mode that contains both C=N and N=N stretching character.

In the Raman spectrum of $[\mathbf{1-H}][\text{AlCl}_4]$, the two bands at 1193 and 1173 cm^{-1} for collapse into a single band located at 1164 cm^{-1} upon ^{15}N substitution.⁷⁷ We suggest that this is because the two signals overlap in the spectrum of the labeled compound. The band located at 1193 cm^{-1} is both sharp and intense in the Raman spectrum, consistent with an N=N stretching mode. Moreover, this

band shifts by 29 cm^{-1} upon isotopic substitution compared with the 40 cm^{-1} shift predicted by a harmonic oscillator model, further supporting the notion that the origin this band is a stretching mode of the N_2 unit. DFT calculations support the description of this vibration as a predominately N=N stretching mode. For $[\mathbf{1-m}]^+$ a band of this type was found at 1148 cm^{-1} which is in close agreement with experimental data given the simplicity of the model system.

Given the wealth of data available for the IR-active, C=N stretching mode of coordinated diazoalkanes, information for the N=N stretching mode remains sparse in comparison to information concerning the same stretch for free diazoalkanes.⁴⁵ The N=N stretching mode of PhC(H)N_2 is 2062 cm^{-1} which is between the values for H_2CN_2 , 2097 cm^{-1} , and Ph_2CN_2 , 2042 cm^{-1} .^{74,78,79} The observed N=N stretch in $[\mathbf{1-H}][\text{AlCl}_4]$ is consistent with a weakening of this bond in comparison to the free diazoalkane.

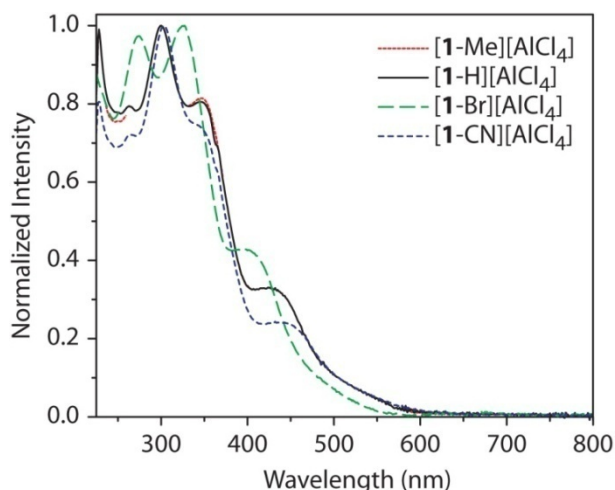


Figure 4. Normalized UV-Vis spectra of $[\mathbf{1-R}][\text{AlCl}_4]$ ($R = \text{Me, H, Br, CN}$) in CH_2Cl_2 at 20 °C.

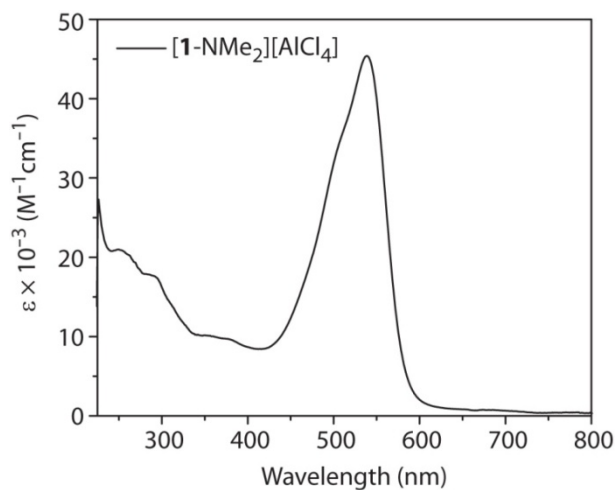


Figure 5. UV-Vis spectrum of $[\mathbf{1-NMe}_2][\text{AlCl}_4]$ in CH_2Cl_2 at 20 °C.

All of the diazoalkane complexes studied have similar vibrational structure (Table 1). In view of the isotopic substitution results obtained for $[\mathbf{1-H}][\text{AlCl}_4]$, the predominantly C=N and N–N stretching modes were located in the IR and Raman spectra for each of $[\mathbf{1-R}][\text{AlCl}_4]$ ($R = \text{NMe}_2, \text{Me}, \text{Br}, \text{CN}$; Table 1). There is no obvious Hammett trend present in the vibrational data, which may reflect the coupling of the multiple vibrational modes. Vibrational modes that have weak intensity in the infrared spectrum were not located for $[\mathbf{1-NMe}_2][\text{AlCl}_4]$ because sample fluorescence interfered with the acquisition of Raman data.

The compounds $[\mathbf{1-R}][\text{AlCl}_4]$ ($R = \text{Me}, \text{H}, \text{Br}, \text{CN}$) are all dark red in color, but solutions of $[\mathbf{1-NMe}_2][\text{AlCl}_4]$ are a vibrant fuchsia color. This observation prompted us to compare the UV-Vis spectral features of these five complexes. The UV-Vis spectra for $[\mathbf{1-R}][\text{AlCl}_4]$ ($R = \text{Me}, \text{H}, \text{Br}, \text{CN}$) all show an absorption near 450 nm and contain no intense absorption bands at lower energies (Figure 4). However, $[\mathbf{1-NMe}_2][\text{AlCl}_4]$ was found to possess an intense absorption with maximum at 538 nm (Figure 5). The absorption band is assigned as a ligand-to-metal charge transfer band (LMCT). This assignment is in accord with both the formally d^0 metal center and the observation that less electron-donating R groups do not give rise to strong absorptions in the visible region. This absorption has a pronounced feature on the hypsochromic side of the band, indicating that the net absorption is the sum of overlapping spectral features. The absorption may be fit to the sum of three Gaussian distributions with spacing of approximately 1180 cm^{-1} . This value likely corresponds to the vibrational mode of the Mo–N bond in the excited state.^{80,81}

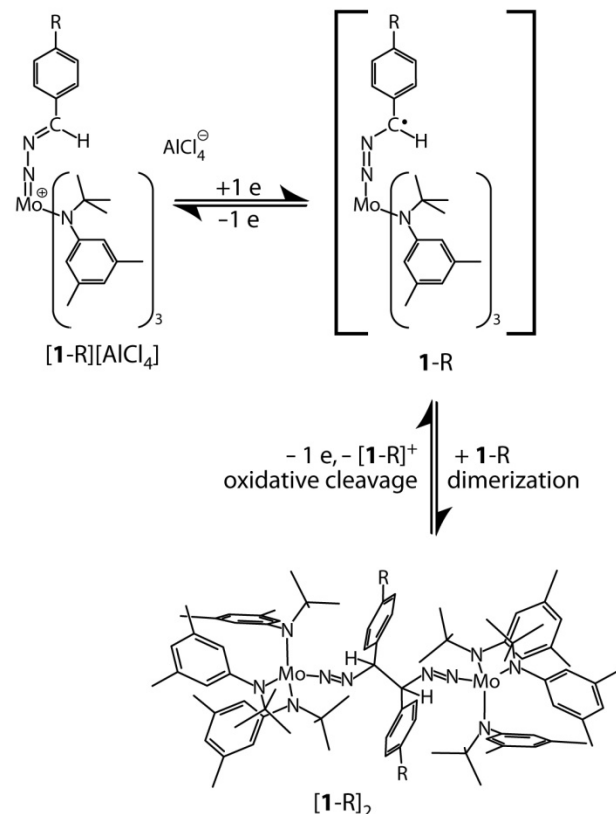
Irradiation of CHCl_3 solutions of $[\mathbf{1-NMe}_2][\text{AlCl}_4]$ with visible light gave rise to an emission with a Stokes shift of 15600 cm^{-1} ($\lambda_{\text{abs}} = 541 \text{ nm}, \lambda_{\text{em}} = 573 \text{ nm}$). A number of workers have recently shown that the LMCT excited state may give rise to fluorescence in d^0 complexes that contain metal-ligand multiple bonds.^{82–84} Our case is distinct in that both absorption and emission of the LMCT excited state occur in the visible region, therefore UV irradiation is not required to observe emission from $[\mathbf{1-NMe}_2][\text{AlCl}_4]$. Indeed, the NMe_2 substituent is found in many efficient organic fluorophores that emit from a CT state.⁸⁵ This is desirable for applications such as photooxidants that may be developed for use with a visible light source.⁸⁴

Reductive Dimerization of Diazoalkane Ligands via C–C Bond Formation. Reduction of the diazoalkane salt, $[\mathbf{1-H}][\text{AlCl}_4]$ by $1e$ was anticipated to generate the odd-electron complex $\text{PhC(H)NNMo(N}[t\text{-Bu}]\text{Ar})_3$, $\mathbf{1-H}$. However, this species was found to be unstable with regard to spontaneous dimerization at carbon to form the dimeric, diazo complex, $\mu\text{-(PhC(H)NN)}_2[\text{Mo(N}[t\text{-Bu}]\text{Ar})_3]_2$, $[\mathbf{1-H}]_2$ (Scheme 2). Addition of solid Cp_2Co to $[\mathbf{1-H}][\text{AlCl}_4]$ dissolved in CHCl_3 leads to the rapid and quantitative formation of $[\mathbf{1-H}]_2$ with precipitation of $[\text{Cp}_2\text{Co}][\text{AlCl}_4]$. Filtration of the reaction mixture removes $[\text{Cp}_2\text{Co}][\text{AlCl}_4]$, leaving only $[\mathbf{1-H}]_2$ in the filtrate which is then collected in 97% yield. This was found to be the most convenient protocol for separating the products despite the observation that Cp_2Co is unstable in CHCl_3 for prolonged periods of time; the formation of $[\mathbf{1-H}]_2$ is essentially complete upon mixing. Dimeric $[\mathbf{1-H}]_2$ has low solubility in solvents such as C_6H_6 , Et_2O , or n -alkanes but forms solutions readily in THF, MeCN, or halocarbons. Upon reduction of $[\mathbf{1-H}][\text{AlCl}_4]$, the characteristic downfield shift at 8.92 ppm in the ^1H

NMR spectrum for the hydrogen atom bound to the diazoalkane carbon moves to 6.17 ppm. This indicates that the unsaturation at that carbon is removed upon reduction, consistent with dimer formation. Examining the ^1H NMR spectrum, it intrigued us that only one set of resonances predominated; one would expect an unselective radical-radical coupling reaction to form a 1:1 mixture of *rac* and *meso* isomers with each isomer having a unique set of chemical shifts. To rationalize this observation, we concluded that the reductive dimerization of $[\mathbf{1-H}][\text{AlCl}_4]$ is selective for the formation of either the *meso* or *rac* product mixtures.

To identify the preferred stereochemistry of C–C bond formation, crystals suitable for X-ray diffraction were grown of $[\mathbf{1-H}]_2$. The molecule crystallizes on a C_2 axis and is therefore assigned as the *rac* isomer (Figure 6). Anomalous scattering data confirmed that the crystallographic model with (*R*, *R*) stereochemistry corresponds to the enantiomer contained within the crystal.^{86–88} The preferential formation of the *rac* isomer is in qualitative agreement with a radical-radical coupling in which a transition state leading to the *rac* product is favored. This is the only transition state that accommodates C–C bond formation with C41–C4–C4'–C41' and N5–C4–C4'–N5' angles that approximate 180° , minimizing unfavorable steric interactions between the two reaction partners. Likewise, reduction of both $[\mathbf{1-Br}][\text{AlCl}_4]$ or $[\mathbf{1-CN}][\text{AlCl}_4]$ with Cp_2Co in d_8 -THF leads to the formation of only one set of signals in the ^1H NMR spectrum which we presume to be the *rac* isomer as for $[\mathbf{1-H}]_2$. However, reduction of $[\mathbf{1-Me}][\text{AlCl}_4]$ or $[\mathbf{1-NMe}_2][\text{AlCl}_4]$ gives mixture of the *meso* and *rac* isomers as judged by ^1H NMR spectroscopy.

Scheme 2



Highly selective formation of the *rac* product for the dimerization of **1-R** (R = H, Br, CN) is consistent with a number of mechanisms. If C–C bond formation were reversible, an equilibrium process involving $[\mathbf{1-R}]_2$ and 2 equiv of **1-R** could drive the dimer to the more stable stereoisomer. However based on the large difference in E_p for $[\mathbf{1-R}]^{0/+}$ and $[\mathbf{1-R}]_2^{0/+}$ of approximately 900 mV (*vide infra*), this explanation appears unlikely. A related scenario is that formation of $[\mathbf{1-R}]_2^+$ by combination of **1-R** and $[\mathbf{1-R}]^+$ is rapid and reversible with respect to the second electron transfer. In such a mechanism, the stereochemical outcome of C–C bond formation might be explained by the relative stability of the two stereoisomers of $[\mathbf{1-R}]_2^+$. An equally plausible possibility is that the two neutral radicals, **1-R**, couple in such a way as to minimize steric repulsion which leads to a preferential formation of *rac* isomers. Electrochemical studies of the pinacol coupling involving 4-substituted acetophenones show a modest preference for the formation of the *rac* isomers in basic media.⁸⁹ Although these results were attributed mainly to hydrogen bonding, similar electrochemical dimerization of benzaldehyde did not discriminate between formation of *rac* or *meso* isomers.^{89,90}

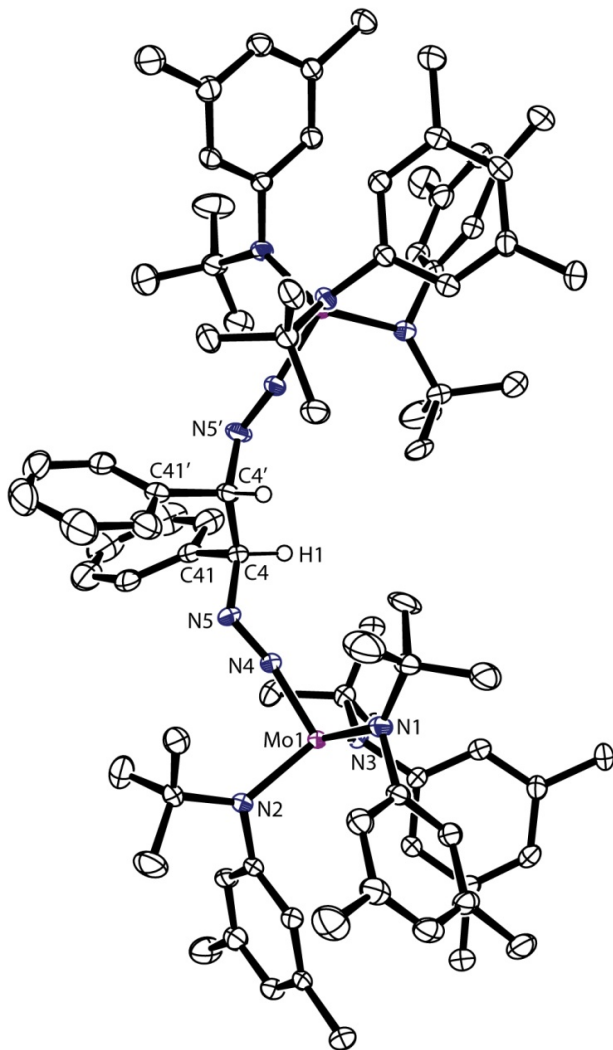
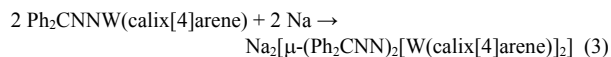
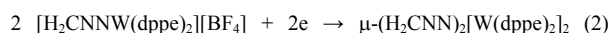
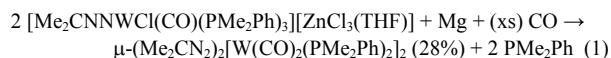


Figure 6. An ORTEP idrawing of $[\mathbf{1-H}]_2$ shown with 50% probability ellipsoids. Hydrogen atoms having calculated atomic positions are omitted for clarity. Selected bond lengths and angles are given in the text.

With respect to $[\mathbf{1-H}][\text{AlCl}_4]$, the C–C bond formation forces the cumulene system to reverse the long and short internuclear distances in $[\mathbf{1-H}]_2$. This structural change occurs in conjunction with the conversion of molybdenum from the +6 to the +4 oxidation state in the reaction during the reductive coupling. The Mo–N distance in $[\mathbf{1-H}]_2$, 1.769(2) Å, is longer than that of $[\mathbf{1-H}][\text{AlCl}_4]$. Correspondingly, the N–N bond is contracted, 1.243(4) Å, and the C–N bond lengthened, 1.478(4) Å, compared to the cationic complex. The newly formed C–C linkage has an internuclear distance of 1.553(6) Å which is typical for such a C–C single bond. In the X-ray crystal structure of $[\mathbf{1-H}]_2$, the N–N–C bond angle of 119.4(3)° is consistent with sp^2 hybridization at nitrogen, as the Mo–N–N angle of 167.2(2)° deviates from linear. This angle is expected to be less than 180° in metal diazenido complexes.⁶² Hoffmann has described the bonding in this functional group (generically, M–N–N–H) and found a codependence of the metal–N–N and N–N–H angles.⁹¹ These calculations concluded that when the latter angle is 120°, the M–N–N angle is predicted to be 174°.

Electrochemical dimerization of coordinated diazoalkanes has been reported for two systems that contain W, eq. 1, 2.^{92,93} In only one case was the product soluble enough for spectroscopic and structural characterization, eq. 1.⁹³ In this case, reduction of $[\text{Me}_2\text{C}(\text{N}=\text{N})\text{WCl}(\text{CO})(\text{PMe}_2\text{Ph})_3]^+$, is accompanied by loss of a phosphine ligand, therefore the reaction was carried out in the presence of CO to cleanly generate the C–C bonded product. Moreover, there is no possibility of forming diastereomeric products because the two faces of the diazoalkane ligand are identical. Reductive dimerization of d^0 diazoalkane complexes of W can also lead to the formation of a W–W bond with the terminal N-atom of the diazoalkane bridging the two W atoms, as opposed to C–C bond formation, eq. 3.⁹⁴



Reductive dimerization of $[\mathbf{1-R}][\text{AlCl}_4]$ proceeds through the intermediacy of the odd-electron, diazoalkane complex **1-R**, that is the initial product of **1e** reduction. Therefore, it seemed natural to interrogate this process by electrochemical methods. Of initial interest was to compare the energy required for reduction of the cation to the neutral radical. A graph of the redox potential versus the Hammett parameter shows a large change in redox potential as a function of the substitution on the 4-R group of the diazoalkane ligand (Figure 7). A fit to the Hammett plot gave a $\rho = -283$ mV for the series R = NMe₂, Me, H, Br, CN. Therefore, complexes having a diazoalkane bearing an electron donating group in the 4-position of the aryl ring deliver a more negative reduction potential than those that contain an electron withdrawing group. A parallel trend has been described for the reduction potential of $[\text{4-R}_6\text{H}_4\text{C}(\text{H})\text{NNM}(\text{dppf})_2\text{F}][\text{BF}_4]$ (M = Mo, W).⁹⁵

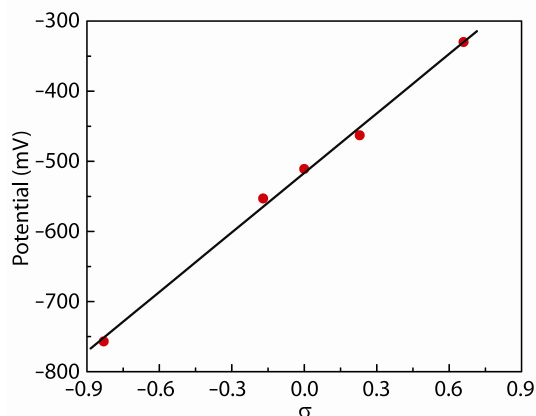


Figure 7. Potentials ($E_{1/2}$ vs. SCE) at which reduction of $[\mathbf{1-R}][\text{AlCl}_4]$ occurs are plotted against the Hammett parameter for R. The fit shown has a $\rho = -283 \text{ mV}$ ($R^2 = 0.998$).

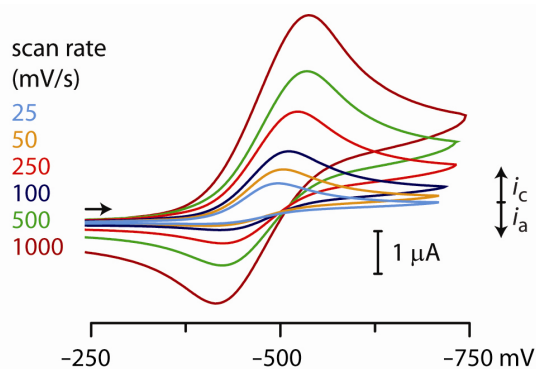


Figure 8. Stack plot of cyclic voltammograms of 1 mM $[\mathbf{1-H}][\text{AlCl}_4]$ in 0.2 M $[\text{N}(n\text{-Bu})_4][\text{PF}_6]/\text{THF}$ solution at 20 °C. Potentials shown are relative to SCE.

In cyclic voltammetry, the ratio of cathodic-to-anodic peak currents reflects the concentration in solution for the generation and decay of electroactive species. Therefore, monitoring this ratio as a function of scan rate is a sensitive marker of how much electroactive species is in solution.⁹⁶ The height of the cathodic wave that produces $\mathbf{1-H}$ varies linearly with the square-root of scan rate – as expected for a 1e reduction (Figure 8).^{96,97} However, the anodic current corresponding to oxidation of $\mathbf{1-H}$ grows in more quickly than predicted by the scan rate variation. This behavior shows that in 1 mM solution $\mathbf{1-H}$ is long-lived enough to be oxidized prior to dimerization at sufficiently fast scan rates. The low anodic peak current for slow scan rates indicates that depletion of $\mathbf{1-H}$ in solution, via dimerization, is fast relative to the timescale of the electrochemical experiment. Consistent with a bimolecular dimerization reaction, cyclic voltammograms of $[\mathbf{1-R}][\text{AlCl}_4]$ were concentration dependent. Increasing the concentration led to less reversible waves while decreasing the concentration gave more reversible behavior.

Solutions of $[\mathbf{1-R}][\text{AlCl}_4]$ ($R = \text{Br}, \text{H}, \text{Me}$) at concentrations of 1 mM have nearly the same cathodic peak current, indicating that the diffusion behavior of the three compounds is similar. A variable

scan rate experiment showed that the ratio of cathodic-to-anodic peak current is not equal for the series (Figure 9). Upon comparing the cyclic voltammograms of $[\mathbf{1-H}][\text{AlCl}_4]$ and $[\mathbf{1-Me}][\text{AlCl}_4]$ under the same conditions (1 mM solutions at a scan rate of 100 mV/s), the wave corresponding to $[\mathbf{1-Me}]^{+/0}$ appears more reversible than that for $[\mathbf{1-H}]^{+/0}$ because the ratio of cathodic-to-anodic peak currents is closer to unity. Assuming that the odd-electron diazoalkane complexes, $\mathbf{1-R}$, have similar diffusion behavior, we would conclude that this ratio should be the same for all three substituents. This result demonstrates that the dimerization process is not diffusion limited.⁹⁸

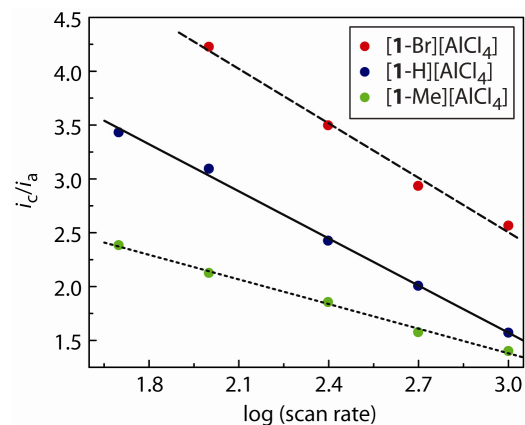


Figure 9. Plots of cathodic/anodic peak currents vs. log of the scan rate (mV/s) show that the dimerization is not diffusion limited. Fits to the data in the form $i_c/i_a = a + b \log(v)$, where v is the scan rate, are shown as follows: $[\mathbf{1-Br}][\text{AlCl}_4]$ (dashed line), $a = 7.56(26)$, $b = -1.69(10)$; $[\mathbf{1-H}][\text{AlCl}_4]$ (solid line), $a = 5.95(10)$, $b = -1.46(4)$; $[\mathbf{1-Me}][\text{AlCl}_4]$ (dotted line), $a = 3.67(6)$, $b = -0.76(3)$.

The dimerization reaction that forms $[\mathbf{1-H}]_2$ as a product by reduction of $[\mathbf{1-H}]^+$ has two limiting mechanisms. Two equiv of the neutral, odd-electron compound $\mathbf{1-H}$ may dimerize forming a C–C bond. Alternatively, $\mathbf{1-H}$ may react with $[\mathbf{1-H}]^+$ to form an intermediate complex $[\mathbf{1-H}]_2^+$ that is subsequently reduced (either by addition of 1e from an electrode or a disproportionation reaction). These two mechanisms may be discriminated by monitoring the changes in the cathodic peak potential as a function of scan rate. In the radical-radical coupling case a slope of -19 is expected for such a plot while a slope of -29 is expected for a radical-cation coupling.^{96,99} Our attempts to make this distinction were not reliable, presumably due to the high resistance of anhydrous media. Except for in the immediate vicinity of the electrode surface, the concentration of $[\mathbf{1-H}]^+$ is always expected to be higher than the concentration of $\mathbf{1-H}$, raising the question as to whether chemical reduction of these cations would necessarily follow the same mechanism that predominates under electrochemical conditions. We favor the notion that this dimerization proceeds by radical-radical coupling, by analogy with the well-studied radical-radical dimerization of the persistent radical, $\text{PhCNMo}(\text{N}[\text{t-Bu}]\text{Ar})_3$,^{53-55,100} but do not rule out a mechanism in which $[\mathbf{1-R}]_2$ is formed by a radical-cation dimerization followed by fast electron transfer.

Savéant has described the electrodimerization of aromatic aldehydes in great detail.^{96,101-105} The mechanism of dimerization has been shown to be a radical-radical coupling of two pinacolate radical anions generated at the electrode. The reaction proceeds at rates much slower than the diffusion limit, and specific solvation by water has a large effect on the measured rate of this reaction.¹⁰⁵ The activation barrier to this reaction has been attributed to entropy requirements in the C–C bond forming step.^{96,102,103} A reduced spin density on the carbon atom brought about by delocalization of the unpaired electron onto the aromatic group both stabilizes the intermediate and raises the entropic requirement for C–C bond formation. Therefore, increasing the amount of radical character at the carbon participating in C–C bond formation generally increases the rate of dimerization.

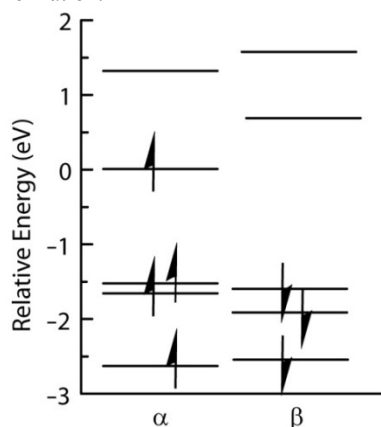


Figure 10. Relative energies of the calculated frontier orbitals for **1-m**.

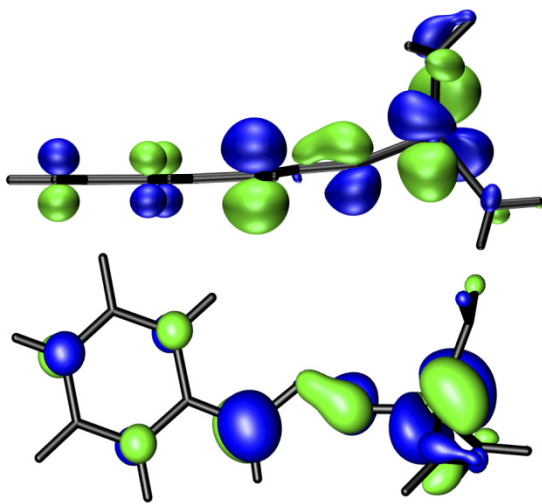


Figure 11. Two views of the SOMO for **1-m** shown at an isosurface value of 0.05.

The transient radical intermediate, **1-H**, is unstable with respect to dimerization to form a C–C bond in the product **[1-H]₂**. Dimerization at carbon suggested to us that the unpaired electron resides partially on the diazoalkane carbon atom. To investigate the electronic structure of the transient radical intermediate, DFT calculations were performed on the model complex

PhC(H)NNMo(NH₂)₃, **1-m**. For a starting geometry the half-molecule that occupies the asymmetric unit in the crystal structure of **[1-H]₂** was used and the anilide ligands were replaced with NH₂ donors. During the geometry optimization, the initially pyramidal diazoalkane carbon atom became planar as expected for an *sp*² hybridization at carbon. In **1-m**, the SOMO is destabilized by approximately 1.5 eV with respect to the SOMO–1 (Figure 10).

Approximately 15% of the SOMO resides on the diazoalkane carbon atom and 43% on Mo (Figure 11). Experimental evidence for the delocalization of unpaired spin density onto diazoalkane ligands has been provided by study of the reduction of [4-RC₆H₄C(H)NNMo(dppe)₂F][BF₄] in an EPR probe.⁹⁵ An EPR resonance centered at *g* = 2.01 was split into a quintet by hyperfine interaction of 2.6 mT from ¹⁴N nuclei. Delocalization of the SOMO of **1-m** onto the aryl ring suggests that a *para* substituent could influence the stability of the SOMO and the relative spin densities for atoms along the diazoalkane fragment. This provides a model for the variation in reduction potential and lifetime of **1-R** with variation of the substituent.

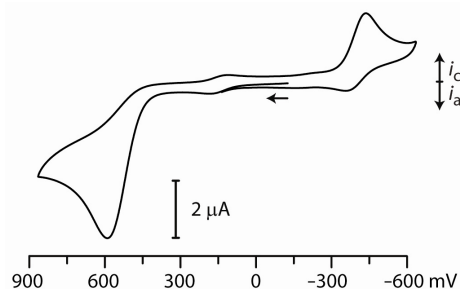


Figure 12. Cyclic voltammogram of **[1-H]₂** in 0.2 M [N(*n*-Bu)₄][PF₆] THF solution acquired at 250 mV/s and 20 °C. Potentials shown are relative to SCE.

Electrochemical oxidation of the dimers **[1-R]₂** gives a broad anodic wave in the cyclic voltammogram with a peak current approximately twice the magnitude of the wave corresponding to the cathodic **[1-R]⁺⁰** couple (Figure 12). Therefore, the oxidation of **[1-R]₂** was assigned as a 2e wave that occurs as a result of two consecutive 1e oxidation events.⁹⁶ Behavior of this kind is expected for an electrochemical oxidation in which the second electron is removed more easily than the first.¹⁰⁶ Consistent with this reasoning is the difference between the oxidation potential of **[1-R]₂** and that of the neutral **1-R**, as the potential of the latter lies approximately 1 V negative of the former. A frequently invoked mechanism for reactions of this type is the *ECE* reaction, wherein oxidation of the dimer, **[1-H]₂**, leads to formation of both **[1-H]⁺** and **1-H** at a potential at which the neutral compound undergoes rapid oxidation to form a second equiv of **[1-H]⁺**.^{99,106}

Interested in the electronic effects of the *para* substituent, we investigated oxidative cleavage for **[1-R]₂**. One would expect that the electronic influence of the substituent to be less dramatic in the case of dimer oxidative cleavage than was observed for reductive coupling of **[1-R]⁺** because of the absence of a conjugated π network enabling communication between the aromatic ring and molybdenum. The potential (*E_p⁺⁰*) for oxidative cleavage of **[1-R]₂** was measured by differential scanning voltammetry and fit to a Hammett plot with a ρ = –160 mV for four points (R = Me, H, Br,

CN; Figure 13). The potential for oxidation of $[1\text{-NMe}_2]_2$ was nearly that of $[1\text{-CN}]_2$. In order to test for a V-shaped Hammett behavior, the compound $[1\text{-OMe}][\text{AlCl}_4]$ was made and briefly investigated. Oxidation of the dimeric species $[1\text{-OMe}]_2$ occurred at $E_p = 417$ mV. This value for $R = \text{OMe}$ fit well to a line when plotted with the other four points ($R = \text{Me}, \text{H}, \text{Br}, \text{CN}$). It is unclear why the potential for $[1\text{-NMe}_2]_2$ does not fit to the Hammett trend, however it is noteworthy that this compound has other nearby oxidation events at more positive potentials that may correspond to oxidation of the dimethylamine functional group (Figure S23).

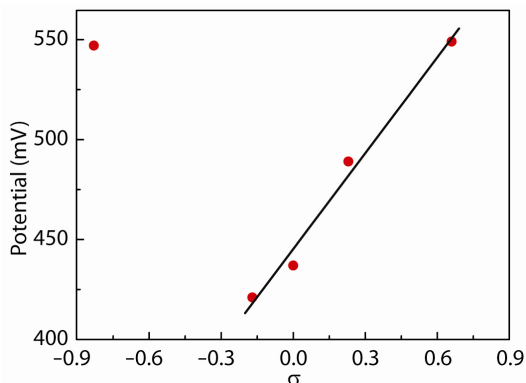
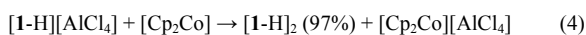


Figure 13. Potentials (E_p vs. SCE) at which oxidative cleavage of $[1\text{-R}]_2$ occur are plotted against the Hammett parameters for R. The fit to four data points has a $\rho = -160$ mV ($R^2 = 0.994$). Data for $[1\text{-NMe}_2]_2$ was not fit to the line.

After the transient radical $\mathbf{1-H}$ dimerizes to form a C–C bond, $2e$ are formally stored in a C–C bond. We sought to engage these electrons in a reaction that would return the starting material, $[1\text{-H}]^+$. Accordingly, oxidative cleavage $[1\text{-H}]_2$ effected by either the addition of AgOTf or $[\text{Cp}_2\text{Fe}][\text{PF}_6]$ to $[1\text{-H}]_2$ give $[1\text{-H}][\text{OTf}]$ (68%) and $[1\text{-H}][\text{PF}_6]$ (78%) as products. This demonstrates a two-step route for conterion exchange that converts the initial diazoalkane complex $[1\text{-H}][\text{AlCl}_4]$ into $[1\text{-H}][\text{A}]$ ($\text{A} = \text{PF}_6^-, \text{OTf}^-$; eq. 4, 5).



Related examples of redox non-innocent C–C bonds have been studied for their capacity to act as charge storage devices. Metallocumulenes such as $\text{Cp}(\text{Et}_2\text{PCH}_2\text{CH}_2\text{PEt}_2)\text{Mn}=\text{C}=\text{CH}_2$ participate in oxidative coupling reactions to form a C–C bonded dimer that formally stores two holes.¹⁰⁷⁻¹⁰⁹ The complementary function, electron storage, is accomplished by $[1\text{-H}]_2$. Combination of hole and electron storing molecules is a goal in the development of molecular batteries.¹⁰⁹ Only a few systems have been described that carry out both functions, such as Floriani's $[\text{M}(\text{salophen})]^n$ ($n = 2, 0, -2$).¹¹⁰⁻¹¹³ Therefore, it has become desirable to find mixed-molecule systems for charge storage. These systems expand the scope of molecular charge storage technology, and make it possible to tune the electrochemical difference between the hole and charge storage compartments of the molecular battery.

Conclusions

A new synthetic route to diazoalkane ligands from N_2 has been described. Characterization of the complexes, $[1\text{-R}][\text{AlCl}_4]$, included Raman spectroscopy to elucidate the N–N stretching frequency of the coordinated diazoalkane, for which literature data are scarce. Reductive dimerization of $[1\text{-R}]^+$ coupled the diazoalkane ligands at carbon to form a bridging ligand. One such dimer, $[1\text{-H}]_2$ was crystallographically characterized. Electrochemical studies showed that reduction of $[1\text{-R}][\text{AlCl}_4]$ forms a transient odd-electron complex, $\mathbf{1-R}$. The structure of this odd-electron intermediate was probed using quantum chemical calculations. Future work might be aimed at liberation of the coordinated diazoalkane from the metal scaffold and the application of C–C coupled diazoalkane ligands in charge storage devices.

Experimental Procedures

General Remarks. All manipulations were carried out under an atmosphere of purified nitrogen in a Vacuum Atmospheres Model MO-40M glovebox equipped with the QP-30 accessory, or by standard Schlenk techniques.^{114,115} Inside the MO-40M glovebox the ambient temperature ranged from 18–22 °C. All glassware was oven-dried at a temperature above 150 °C for at least 12 hours and allowed to cool under dynamic vacuum prior to use. Celite, alumina, and 4 Å sieves were activated by heating to a temperature greater than 180 °C under a dynamic vacuum for 2 d (Celite) or 5 d (alumina and 4 Å sieves). Et_2O , *n*-hexane, *n*-pentane, and toluene were bubble degassed with nitrogen and forced, under positive pressure, through a column of activated alumina followed by a column of activated Q5.¹¹⁶ CH_2Cl_2 was bubble degassed with nitrogen and forced, under positive pressure, through two columns of activated alumina.¹¹⁶ THF was dried over sodium metal and distilled from dark purple solutions of sodium benzophenone ketyl. MeCN was taken from an Aldrich Sure-Seal bottle, filtered through a column of activated alumina (4×3 cm), and degassed under a dynamic vacuum. $\text{O}(\text{SiMe}_3)_2$ was distilled from dark purple solutions of sodium benzophenone ketyl. CHCl_3 was refluxed over CaH_2 for 48 h prior to distillation. All solvents were stored over 4 Å sieves. C_6D_6 was degassed by three freeze-pump-thaw cycles and stored over 4 Å sieves for 3 d prior to use. CDCl_3 and CD_2Cl_2 were refluxed over CaH_2 for 24 h then distilled and stored over 4 Å sieves. ^1H and ^{13}C NMR shifts are referenced to residual solvent resonances (for CD_2Cl_2 5.32 ppm and 54.00 ppm). All ^{15}N NMR spectra are externally referenced to neat $\text{H}_3\text{CC}^{15}\text{N}$ ($\delta = 245$ ppm) in comparison to liquid NH_3 ($\delta = 0$ ppm).¹¹⁷ UV-Vis spectra were obtained on HP8453 spectrophotometers in 1 cm quartz cells manufactured by Starna. Infrared spectra were obtained on a Nicolet Magna 860 FT-IR in transmission mode. Positive ion ESI-MS were obtained using a Bruker Daltonics APEXIV, 4.7 T Fourier Transform Ion Cyclotron Resonance Mass Spectrometer. Combustion analysis was performed by Midwest MicroLab, LLC (Indianapolis, IN).

Raman Spectroscopy. An Invictus solid state laser at 785 nm manufactured by Kaiser Optics was routed through fiber optic cables to a Hololab series 5000 Raman Microscope. The sample was placed in an NMR tube under the objective (10×) of the microscope. The Stokes shifted Raman scattering was observed via

180° reflectance through the objective of the Raman microscope at a laser power of 30 mW. Reported Raman spectra are an average of 8 spectra, each collected for 2 s using an automated routine in Hololab software to automatically correct for the dark current. The averaged spectrum has the solvent signals subtracted and was subsequently baseline corrected using GRAMS software. Raman shifts are reported in reference to an external standard of neat cyclohexane (801.3 cm⁻¹).

Electrochemical Measurements. A Bioanalytic Systems CW-50 potentiostat, 1 mm diameter Pt disk working electrode, Pt wire counter electrode, and Ag wire pseudo-reference electrode were used for all measurements. All electrochemical measurements were made in 0.2 M [N(*n*-Bu)₄][PF₆] THF solutions. To measure potentials, Cp*₂Fe was used as an internal standard. The Cp*₂Fe^{0/+} couple is referenced to 117 mV vs SCE. Reversible redox potentials of [1-R][AlCl₄] were measured by cyclic voltammetry of 50 μM solution at several scan rates. Oxidative peak potentials of in situ formed [1-R]₂ were measured by differential pulse voltammetry (dpv) acquired on 5 mM solutions of [1-R][AlCl₄]. DPV data were acquired with a single scan from ca. -1 V to 1 V taken at 20 mV/s using the following data collection parameters: pulse height, 50 mV; pulse length, 50 ms; sampling intervals, 20 ms; and cycle repeat time, 200 ms. For R = OMe, all potentials were measured at arbitrary concentrations. Isolated samples of [1-H][AlCl₄] and [1-H]₂ show the same features in the cyclic voltammogram.

Single Crystal X-ray Diffraction. X-ray diffraction data were collected using a Siemens Platform three-circle diffractometer coupled to a Bruker-AXS Smart Apex CCD detector with graphite-monochromated Mo K α radiation ($\lambda = 0.71073 \text{ \AA}$), performing ϕ - and ω -scans. The molecular structure was obtained by direct methods using SHELXS¹¹⁸ and refined against F^2 on all data by full-matrix least squares with SHELXL-97^{119,120}. All non-hydrogen atoms were refined anisotropically; all hydrogen atoms were included into the model at their geometrically calculated positions and refined using a riding model except for the hydrogen atom labeled H1 in the structures for [1-H][AlCl₄], [1-NMe₂][AlCl₄], and [1-H]₂. The atom labeled H1 was located in a Fourier difference map and the C-H distance was refined upon.

Quantum Chemical Calculations. All density functional theory (DFT) calculations were carried out using the Amsterdam Density Functional (ADF) program package, versions 2004.01 or 2008.01.¹²¹⁻¹²³ The geometry of 1-m was optimized using the local exchange-correlation potential of Vosko *et al.*¹²⁴ (VWN) augmented self-consistently with gradient-corrected functionals for electron exchange according to Becke¹²⁵ and for electron correlation according to Perdew.^{126,127} This nonlocal density functional is termed BP86 in the literature.¹²⁸ All other calculations were carried out using the OLYP functional which is a combination of the OPTX exchange functional of Handy and Cohen used with Lee, Yang, and Parr's nonlocal correlation function (LYP).¹²⁹⁻¹³¹ For all calculations, relativistic effects were included using the zero-order regular approximation (ZORA).^{132,133} The basis set used was the all-electron ADF ZORA/TZ2P (triple ζ with two polarization functions) basis. NMR spectroscopy chemical shifts and coupling constants were obtained from optimized geometries of the full molecules [1-H]⁺ and [1-H]₂. Crystallographically determined atomic

positions were used as the starting point for all geometry optimizations.

¹⁵N NMR data for ¹⁵N₂-Me₃SiNNMo(N[*t*-Bu]Ar)₃. This compound was prepared from Mo(N[*t*-Bu]Ar)₃ and ¹⁵N₂ following literature procedures.¹⁶ ¹⁵N{¹H} NMR (50 MHz, CDCl₃, 20 °C): $\delta = 400$ (d, ¹J_{NN} = 12 Hz, NMo), 278 (d, ¹J_{NN} = 12 Hz, NSi). Identical chemical shifts and coupling constants were obtained at 50 MHz and 20 °C in C₆D₆. When ¹H decoupling is not applied the resonance at 280 ppm is unobserved, consistent with weakened intensity when the resonance is split by the protons on the trimethylsilyl group.

Preparation of [4-RC₆H₄C(H)NNMo(N[*t*-Bu]Ar)₃][AlCl₄], [1-R][AlCl₄].

The procedure used for [1-H][AlCl₄] is given. Minor modifications of this procedure were used in the synthesis of all other diazoalkane salts, [1-R][AlCl₄], discussed herein. See Supporting Information for complete preparative details.

At 20 °C, 5 mL Et₂O was added dropwise to a stirred suspension of AlCl₃ (755 mg, 5.655 mmol, 2.08 equiv) in 10 mL *n*-pentane to form a solution. The so obtained solution was then added dropwise to a mixture of Me₃SiNNMo(N[*t*-Bu]Ar)₃ (2.00 g, 2.755 mmol) and PhCHO (293 mg, 2.764 mmol, 1 equiv) in 80 mL Et₂O. Upon addition, a red precipitate formed. The mixture was additionally stirred for 2 h before the solids were collected by filtration of the reaction mixture. The so obtained solids were washed with Et₂O (15 mL \times 6) to remove a yellow filtrate. Drying of the solids under a dynamic vacuum afforded the product as a red powder (2.333 g, 2.491 mmol, 90.4%). Crystals suitable for X-ray diffraction studies were grown from THF/*n*-pentane at -35 °C. Characterization data is listed below.

Characterization Data for [4-Me₂NC₆H₄C(H)NNMo(N[*t*-Bu]Ar)₃][AlCl₄], [1-NMe₂][AlCl₄]. ¹H NMR (600 MHz, CDCl₃, 20 °C): $\delta = 8.56$ (1 H, s, CHN₂), 7.84 (2 H, br, Me₂NC₃H₂), 6.98 (3 H, s, *para*-Ar), 6.81 (2 H, d, H₂C₃C(H)N₂), 5.78 (6 H, s, *ortho*-Ar), 3.24 (6 H, s, NCH₃), 2.18 (18 H, s, Ar-CH₃), 1.26 (27 H, s, C(CH₃)₃) ppm. ¹³C NMR (125 MHz, CDCl₃, 20 °C): $\delta = 163.8$ (N₂C), 156.1 (Me₂NC), 145.5 (*ipso*-Ar), 138.6, 130.7, 129.3, 116.6, 112.9, 68.0 (CMe₃), 40.7 (NMe₂), 32.2 (CMe₃), 21.6 (Ar-Me) ppm; one carbon was obscured. ²⁷Al NMR (125 MHz, CDCl₃, 20 °C): $\delta = 103.4$ ppm. ESI-MS: $m/z = 787.4348$ (787.4339, M⁺). Anal. Calcd for C₄₅H₆₅N₆MoAlCl₄: C, 56.61; H, 6.86; N, 8.80; Cl, 14.85. Found: C, 56.42; H, 6.84; N, 8.85; Cl, 14.83. UV-Vis: λ (ϵ) = 538 (45400), 509 (35300, shoulder) nm (M⁻¹cm⁻¹). MP = 125-135 °C (dec).

Characterization Data for [4-MeOC₆H₄C(H)NNMo(N[*t*-Bu]Ar)₃][AlCl₄], [1-OMe][AlCl₄]. ¹H NMR (600 MHz, CDCl₃, 20 °C): $\delta = 8.78$ (1 H, s, CHN₂), 8.03 (2 H, d, H₂C₃C(H)N₂), 7.10 (2 H, d, MeOC₃H₂), 7.00 (3 H, s, *para*-Ar), 5.74 (6 H, s, *ortho*-Ar), 3.94 (3H, s, OCH₃), 2.18 (18 H, s, Ar-CH₃), 1.26 (27 H, s, C(CH₃)₃) ppm. ¹³C NMR (125 MHz, CDCl₃, 20 °C): $\delta = 166.4$ (MeOC), 164.8 (N₂C), 145.2 (*ipso*-Ar), 138.7, 133.4, 130.9, 128.9, 122.0, 115.8, 68.8 (CMe₃), 56.2 (OMe), 32.0 (CMe₃), 21.3 (Ar-Me) ppm. ²⁷Al NMR (125 MHz, CDCl₃, 20 °C): $\delta = 103.4$ ppm. Anal. Calcd for C₄₄H₆₂AlCl₄MoN₅O: C, 56.12; H, 6.64; N, 7.44; Cl, 15.05. Found: C, 55.86; H, 6.26; N, 7.53; Cl, 15.00%.

Characterization Data for [4-MeC₆H₄C(H)NNMo(N[*t*-Bu]Ar)₃][AlCl₄], [1-Me][AlCl₄]. ¹H NMR (600 MHz, CDCl₃, 20 °C): $\delta = 8.87$ (1 H, s, CHN₂), 7.96 (2 H, d, H₂C₃C(H)N₂), 7.40 (2

H, d, MeC₃H₂), 7.02 (3 H, s, *para*-Ar), 5.75 (6 H, s, *ortho*-Ar), 2.50 (3 H, s, C₆H₄CH₃), 2.19 (18 H, s, Ar-CH₃), 1.28 (27 H, s, C(CH₃)₃) ppm. ¹³C NMR (125 MHz, CDCl₃, 20 °C): δ = 165.6 (N₂C), 147.7, 145.3 (*ipso*-Ar), 138.8, 131.0, 131.0, 130.8, 128.9, 127.5, 69.2 (CMe₃), 32.1 (CMe₃), 22.5 (C₆H₄Me), 21.6 (Ar-Me) ppm. ²⁷Al NMR (125 MHz, CDCl₃, 20 °C): δ = 103.4 ppm. ESI-MS: *m/z* = 758.4081 (758.4073, M⁺). Anal. Calcd for C₄₄H₆₂AlCl₄MoN₅: C, 57.06; H, 6.75; N, 7.57; Cl, 15.12. Found: C, 57.03; H, 6.76; N, 7.36; Cl, 14.78%. MP = 191-193 °C.

Characterization Data for [PhC(H)NNMo(N[*t*-Bu]Ar)₃][AlCl₄], [1-H][AlCl₄].

¹H NMR (600 MHz, CDCl₃, 20 °C): δ = 8.96 (1 H, s, CHN₂), 8.10 (2 H, d, *ortho*-Ph), 7.70 (1 H, t, *para*-Ph), 7.61 (2 H, t, *meta*-Ph), 7.04 (3 H, s, *para*-Ar), 5.75 (6 H, s, *ortho*-Ar), 2.20 (18 H, s, Ar-CH₃), 1.29 (27 H, s, C(CH₃)₃) ppm. ¹³C NMR (125 MHz, CDCl₃, 20 °C): δ = 165.5 (NNC), 145.3 (*ipso*-Ar), 135.8, 131.1, 130.9, 130.9, 130.2, 129.9, 128.8, 69.4 (CMe₃), 32.1 (CMe₃), 21.6 (Ar-CH₃) ppm. ²⁷Al NMR (125 MHz, CDCl₃, 20 °C): δ = 103.4 ppm. ESI-MS: *m/z* = 744.3939 (744.3917, M⁺). Anal. Calcd for C₄₃H₆₀AlCl₄MoN₅: C, 56.62; H, 6.64; N, 7.68; Cl, 15.35. Found: C, 56.77; H, 6.73; N, 7.36; Cl, 15.33%. For ¹⁵N₂-[1-H][AlCl₄], ¹⁵N NMR (50 MHz, CDCl₃, 20 °C): 384 (*dd*, ¹J_{NN} = 17 Hz, ²J_{NH} = 3 Hz, Mo-N), 417 (*dd*, ¹J_{NN} = 17 Hz, ³J_{NH} = 6 Hz, N-C) ppm. MP = 192-194 °C.

Characterization Data for [4-BrC₆H₄C(H)NNMo(N[*t*-Bu]Ar)₃][AlCl₄], [1-Br][AlCl₄]. ¹H NMR (600 MHz, CDCl₃, 20 °C): δ = 8.98 (1 H, s, CHN₂), 8.00 (2 H, d, H₂C₃CHN₂), 7.73 (2 H, d, H₂C₃Br), 7.02 (3 H, s, *ortho*-Ar), 5.75 (6 H, s, *para*-Ar), 2.20 (18 H, s, Ar-CH₃), 1.28 (27 H, s, C(CH₃)₃) ppm. ¹³C NMR (125 MHz, CDCl₃, 20 °C): δ = 164.4 (NNC), 145.3 (*ipso*-Ar), 138.8, 133.3, 132.0, 131.1, 131.0, 128.9 (C-Br), 128.8, 69.5 (CMe₃), 32.1 (CMe₃), 21.6 (Ar-Me) ppm; one carbon was obscured. ²⁷Al NMR (125 MHz, CDCl₃, 20 °C): δ = 103.4 ppm. ESI-MS: *m/z* = 822.3026 (822.3022, M⁺). Anal. Calcd for C₄₃H₅₉AlBrCl₄MoN₅: C, 52.17; H, 6.01; N, 7.07; Br, 7.97; Cl, 14.14. Found: C, 51.79; H, 5.92; N, 6.97; Br, 7.57; Cl, 13.43%. MP = 189-192 °C.

Preparation of [4-NCC₆H₄C(H)NNMo(N[*t*-Bu]Ar)₃][AlCl₄], [1-CN][AlCl₄]. ¹H NMR (600 MHz, CDCl₃, 20 °C): δ = 9.12 (1 H, s, CHN₂), 8.28 (2 H, d, H₂C₃CHN₂), 7.84 (2 H, d, H₂C₃CN), 7.03 (6 H, s, *para*-Ar), 5.75 (6 H, s, *ortho*-Ar), 2.20 (18 H, s, Ar-CH₃), 1.29 (27 H, s, C(CH₃)₃) ppm. ¹³C NMR (125 MHz, CDCl₃, 20 °C): δ = 163.0 (N₂C), 145.3 (*ipso*-Ar), 138.9 br, 134.6 br, 133.6, 131.2, 130.9, 128.5, 69.9 (CMe₃), 32.0 (CMe₃), 21.6 (Ar-Me) ppm; one carbon was obscured. ²⁷Al NMR (125 MHz, CDCl₃, 20 °C): δ = 103.4 ppm. ESI-MS: *m/z* = 769.3870 (769.3869, M⁺). Anal. Calcd for C₄₄H₅₉AlCl₄MoN₆: C, 56.39; H, 6.35; N, 8.97; Cl, 14.94. Found: C, 56.04; H, 6.40; N, 8.65; Cl, 14.71%. MP = 112-120 °C (dec).

Thermal Stability of [PhC(H)NNMo(N[*t*-Bu]Ar)₃][AlCl₄], [1-H][AlCl₄]. Into 1.0 mL of CDCl₃ was dissolved [1-H][AlCl₄] (50 mg, 0.055 mmol) to form a red solution. The solution was then heated to 50 °C for 5 d over which time no color change was observed. Analysis by ¹H NMR spectroscopy showed only [1-H][AlCl₄], and no evidence of decomposition.

Preparation of μ-(PhC(H)NN)₂[Mo(N[*t*-Bu]Ar)₃]₂, [1-H]₂. At -35 °C a solution of [1-H][AlCl₄] (1.00g, 1.24 mmol) in 30 mL CHCl₃ was added Cp₂Co (234 mg, 1.24 mmol, 1 equiv) as a solid. The vessel that contained Cp₂Co was rinsed with 10 mL of *n*-

pentane that was also added to the reaction mixture. The resulting mixture rapidly changed in color from the initial dark red to yellow. The mixture was stirred for 20 min while warming to 20 °C. Filtration of the reaction mixture through celite removed yellow solids that were washed with *n*-pentane (30 mL × 2). The filtrate was then filtered through celite a second time and the solvent removed under a dynamic vacuum. The dried filtrate was collected as a yellow powder (764 mg, 1.20 mmol, 96.7%), mp = 156-160 °C (dec). ¹H NMR (500 MHz, CDCl₃, 20 °C): δ = 7.28 (4 H, t, *meta*-Ph), 7.20 (6 H, m, *ortho*- and *para*-Ph), 6.74 (6 H, s, *para*-Ar), 6.16 (2 H, s, CHN₂), 5.73 (12 H, s, *ortho*-Ar), 2.10 (36 H, s, Ar-CH₃), 1.27 (54 H, s, C(CH₃)₃) ppm. ¹H NMR (500 MHz, *d*₈-THF, 20 °C): δ = 7.28 (4 H, t, *meta*-Ph), 7.13 (6 H, m, *ortho*- and *para*-Ph), 6.75 (6 H, s, *para*-Ar), 6.2 (2 H, s, CHN₂), 5.78 (12 H, s, *ortho*-Ar), 2.09 (36 H, s, Ar-CH₃), 1.26 (54 H, s, C(CH₃)₃) ppm. ¹³C NMR (125 MHz, CDCl₃, 20 °C): δ = 149.1 (*ipso*-Ar), 141.6, 136.8, 130.9, 130.1, 127.5, 126.1, 126.0, 73.8 (CMe₃), 62.4 (N₂C), 32.9 (CMe₃), 21.4 (Ar-Me) ppm. FT-IR (CDCl₃, 20 °C): ν_{NN} = 1453 cm⁻¹. Anal. Calcd for C₈₆H₁₂₀Mo₂N₁₀: C, 69.52; H, 8.14; N, 9.43. Found: C, 69.34; H, 8.19; N, 9.36. A single crystal suitable to X-ray crystallographic analysis was obtained by storing a THF solution at -35 °C for several days. For ¹⁵N₄-[1-H]₂: ¹⁵N NMR (50 MHz, CDCl₃, 20 °C): 428 (*d*, ¹J_{NN} = 17 Hz, NMo), 304 (*d*, ¹J_{NN} = 17 Hz, NC) ppm.

Preparation of μ-(4-RC₆H₄C(H)NN)₂[Mo(N[*t*-Bu]Ar)₃]₂, [1-R]₂, by Cp₂Co reduction of [4-R-C₆H₄C(H)NNMo(N[*t*-Bu]Ar)₃][AlCl₄], [1-R][AlCl₄]. Into 0.5 mL of *d*₈-THF was dissolved [1-R][AlCl₄] to form a red solution. To this solution was added to approx 1 equiv of Cp₂Co in the proportions given below. Upon addition the solution took on a yellow hue immediately, and a light yellow precipitate formed, presumably [Cp₂Co][AlCl₄] after stirring the mixture for 3 min. The reaction mixture was filtered and the filtrate analyzed by ¹H NMR spectroscopy. For [1-NMe₂][AlCl₄] (50 mg, 0.052 mmol) and Cp₂Co (10 mg, 0.054 mmol). ¹H NMR (500 MHz, *d*₈-THF, 20 °C): δ = 7.12 (4 H, d, Me₂NC₃H₂), 6.74 (6 H, s, *para*-Ar), 6.55 (4 H, d, H₂C₃C(H)N₂), 6.09 (2 H, s, CHN₂), 5.76 (12 H, s, *ortho*-Ar), 2.91 (6 H, s, Me), 2.08 (36 H, s, Ar-CH₃), 1.28 (54 H, s, C(CH₃)₃) ppm and δ = 7.66 (4 H, d, Me₂NC₃H₂), 7.31 (4 H, d, H₂C₃C(H)N₂), 6.74 (6 H, s, *para*-Ar), 5.25 (2 H, s, CHN₂), 5.74 (12 H, s, *ortho*-Ar), 2.93 (6 H, s, Me), 2.07 (36 H, s, Ar-CH₃), 1.29 (54 H, s, C(CH₃)₃) ppm formed in a 1.0:0.4 ratio. For [1-Me][AlCl₄] (48 mg, 0.052 mmol) and Cp₂Co (10 mg, 0.054 mmol). ¹H NMR (500 MHz, *d*₈-THF, 20 °C): δ = 7.50 (4 H, br s, MeC₃H₂), 7.15 (6 H, s, *para*-Ar), 6.96 (4 H, s, H₂C₃C(H)N₂), 6.14 (2 H, s, CHN₂), 5.84 (6 H, s, C₆H₄CH₃), 5.78 (12 H, s, *ortho*-Ar), 2.09 (36 H, s, Ar-CH₃), 1.26 (54 H, s, C(CH₃)₃) ppm and δ = 7.37 (4 H, br s, MeC₃H₂), 7.08 (6 H, s, *para*-Ar), 6.75 (4 H, s, H₂C₃C(H)N₂), 6.32 (2 H, s, CHN₂), 5.84 (6 H, s, C₆H₄CH₃), 5.78 (12 H, s, *ortho*-Ar), 2.24 (36 H, s, Ar-CH₃), 1.35 (54 H, s, C(CH₃)₃) ppm formed in a 1.0:0.85 ratio. For [1-H][AlCl₄] (50 mg, 0.053 mmol) and Cp₂Co (11 mg, 0.058 mmol). ¹H NMR data are identical to that given above. For [1-Br][AlCl₄] (52 mg, 0.053 mmol) and Cp₂Co (10 mg, 0.054 mmol). ¹H NMR (500 MHz, *d*₈-THF, 20 °C): δ = 7.33 (4 H, br s, BrC₃H₂), 7.22 (4 H, s, H₂C₃C(H)N₂), 6.76 (6 H, s, *para*-Ar), 6.13 (2 H, s, CHN₂), 5.73 (12 H, s, *ortho*-Ar), 2.09 (36 H, s, Ar-CH₃), 1.26 (54 H, s, C(CH₃)₃). For [1-CN][AlCl₄] (50 mg, 0.053 mmol) and Cp₂Co (11 mg, 0.058 mmol). ¹H NMR (500 MHz, *d*₈-THF, 20 °C): δ = 7.54

(4 H, br s, NCC_3H_2), 7.43 (4 H, s, $\text{H}_2\text{C}_3\text{C}(\text{H})\text{N}_2$), 6.79 (6 H, s, *para*-Ar), 6.32 (2 H, s, CHN_2), 5.78 (12 H, s, *ortho*-Ar), 2.10 (36 H, s, Ar- CH_3), 1.26 (54 H, s, $\text{C}(\text{CH}_3)_3$).

Oxidative Cleavage of μ -(PhC(H)NN) $_2$ [Mo(N(*t*-Bu)Ar) $_3$] $_2$, [I-H] $_2$, by [Cp $_2$ Fe][PF $_6$]. A 5 mL THF solution of [I-H] $_2$ (300 mg, 202 mmol) was frozen in a liquid nitrogen-cooled cold well. To the frozen solution was added [Cp $_2$ Fe][PF $_6$] (135 mg, 408 mmol, 2 equiv) as a solid. Upon thawing of the initially yellow solution, an immediate color change to red-orange occurred. The mixture was allowed to stir at 20 °C for 20 min. The mixture was filtered through celite and the celite pad was washed with 5 mL of THF. The combined filtrate was dried under a dynamic vacuum to afford a red-orange powder. The powder was stirred in 15 mL *n*-pentane at 20 °C for 15 min to form a yellow solution, presumably containing the Cp $_2$ Fe byproduct, that was removed by filtration. The red solids that remained atop the frit were washed with *n*-pentane (5 mL \times 2) until the washings were colorless, and dried under a dynamic vacuum (280 mg, 315 mmol, 78%), mp = 186–192 °C (dec). ^1H NMR data is identical to that reported for [I-H][AlCl $_4$]. ^{19}F NMR (376 MHz, CDCl $_3$, 20 °C): δ = -73 (d, $^1J_{\text{FP}}$ = 715 Hz) ppm. ^{31}P NMR (162 MHz, CDCl $_3$, 20 °C): δ = -144 (sept, $^1J_{\text{PF}}$ = 715 Hz) ppm.

Oxidative Cleavage of μ -(PhC(H)NN) $_2$ [Mo(N(*t*-Bu)Ar) $_3$] $_2$, [I-H] $_2$, by AgOTf. The [I-H] $_2$ (45.1 mg, 0.0304 mmol) was dissolved in Et $_2$ O (20 mL). To the solution was added AgOTf (15.6 mg, 0.0607 mmol) and the mixture was stirred for 2 h at room temperature. The mixture was filtered and the volatiles in the filtrate were removed in vacuo. Crystallization from benzene/THF layered with *n*-pentane gave bright orange microcrystals of [(PhCHNN)Mo(N(*t*-Bu)Ar) $_3$][OTf] (37.0 mg, 68% yield). ^1H NMR data is identical to that reported for [I-H][AlCl $_4$]. ^{19}F NMR (282 MHz, CDCl $_3$, 20 °C): -76.9 ppm. Anal. Calcd for C $_{44}\text{H}_{60}\text{F}_3\text{MoN}_5\text{O}_3\text{S}$: C, 59.25; H, 6.78; N, 7.85; Found: C, 59.01; H, 6.63; N, 7.65.

Acknowledgment. Emily McLaurin is thanked for acquiring the fluorescence spectrum of [I-NMe $_2$][AlCl $_4$]. We thank Professor Daniel G. Nocera for insightful discussions and experimental assistance. Professors Bill Geiger and Jean-Michel Savéant are thanked for helpful discussions. We gratefully thank the NSF for funding this work (Grant CHE-719157).

Supporting Information Available: ESI-MS, ^1H NMR, IR, Raman and CV data for compounds [I-R][AlCl $_4$] in addition to computational details are included in the supporting information. This material is available free of charge via the Internet at <http://pubs.acs.org>.

References:

[†] Current address: Department of Applied Chemistry, Graduate School of Engineering, Osaka University, Suita, Osaka, 565-0871, Japan.

*To whom correspondence should be addressed: cummins@mit.edu

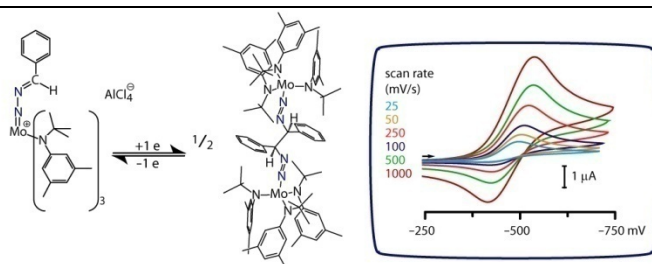
1. Hidai, M.; Mizobe, Y. *Chem. Rev.* **1995**, *95*, 1115-1133.
2. Hidai, M.; Mizobe, Y. *Can. J. Chem.* **2005**, *83*, 358-374.
3. Schrock, R. R. *Acc. Chem. Res.* **2005**, *38*, 955-962.

4. Yandulov, D. V.; Schrock, R. R. *Science* **2003**, *301*, 76-78.
5. Gilbertson, J. D.; Szymczak, N. K.; Tyler, D. R. *J. Am. Chem. Soc.* **2005**, *127*, 10184-10185.
6. Pool, J. A.; Lobkovsky, E.; Chirik, P. J. *Nature* **2004**, *427*, 527-530.
7. MacKay, B. A.; Fryzuk, M. D. *Chem. Rev.* **2004**, *104*, 385-401.
8. Gruber, N.; Galloway, J. N. *Nature* **2008**, *451*, 293-296.
9. Hori, K.; Mori, M. *J. Am. Chem. Soc.* **1998**, *120*, 7651-7652.
10. Hori, M.; Mori, M. *J. Org. Chem.* **1995**, *60*, 1480-1481.
11. Curley, J. J.; Sceats, E. L.; Cummins, C. C. *J. Am. Chem. Soc.* **2006**, *128*, 14036-14037.
12. MacKay, B. A.; Munha, R. F.; Fryzuk, M. D. *J. Am. Chem. Soc.* **2006**, *128*, 9472-9483.
13. Morello, L.; Love, J. B.; Patrick, B. O.; Fryzuk, M. D. *J. Am. Chem. Soc.* **2004**, *126*, 9480-9481.
14. Fryzuk, M. D.; MacKay, B. A.; Patrick, B. O. *J. Am. Chem. Soc.* **2003**, *125*, 3234-3235.
15. Fryzuk, M. D.; MacKay, B. A.; Johnson, S. A.; Patrick, B. O. *Angew. Chem., Int. Ed.* **2002**, *41*, 3709-3712.
16. Figueroa, J. S.; Piro, N. A.; Clough, C. R.; Cummins, C. C. *J. Am. Chem. Soc.* **2006**, *128*, 940-950.
17. Hidai, M.; Mizobe, Y.; Sato, M.; Kodama, T.; Uchida, Y. *J. Am. Chem. Soc.* **1978**, *100*, 5740-5748.
18. Hidai, M.; Ishii, Y. *Bull. Chem. Soc. Jpn.* **1996**, *69*, 819-831.
19. Bernskoetter, W. H.; Olmos, A. V.; Pool, J. A.; Lobkovsky, E.; Chirik, P. J. *J. Am. Chem. Soc.* **2006**, *128*, 10696-10697.
20. Mizobe, Y.; Ishii, Y.; Hidai, M. *Coord. Chem. Rev.* **1995**, *139*, 281-311.
21. Houk, K. N.; Sims, J.; Duke, R. E.; Strozier, R. W.; George, J. K. *J. Am. Chem. Soc.* **1973**, *95*, 7287-7301.
22. Rolf, H. *Angew. Chem. Int. Ed.* **1963**, *2*, 565-598.
23. Andrews, S. D.; Day, A. C.; McDonald, A. N. *J. Chem. Soc. C* **1969**, 787-790.
24. Huisgen, R.; Eberhard, P. *Tet. Lett.* **1971**, *12*, 4343-4346.
25. Guerra, F. M.; Mish, M. R.; Carreira, E. M. *Org. Lett.* **2000**, *2*, 4265-4267.
26. Cunico, R. F.; Lee, H. M. *J. Am. Chem. Soc.* **1977**, *99*, 7613-7622.
27. Jones, W. M.; Glenn, T. H.; Baarda, D. G. *J. Org. Chem.* **1963**, *28*, 2887-2889.
28. Bauer, U.; Egner, B. J.; Nilsson, I.; Berghult, M. *Tet. Lett.* **2000**, *41*, 2713-2717.
29. Adams, J. L.; Gallagher, T.; Osifo, I. K. *Pyrazole and Pyrazoline Substituted Compounds* **2004**, Patent US 6774127.
30. Bevan, P. C.; Chatt, J.; Hidai, M.; Leigh, G. J. *J. Organomet. Chem.* **1978**, *160*, 165-176.
31. Ben-Shoshan, Chatt, J.; Hussain, W.; Leigh, G. J. *J. Organomet. Chem.* **1976**, *112*, C9-C10.
32. Hidai, M.; Mizobe, Y.; Uchida, Y. *J. Am. Chem. Soc.* **1976**, *98*, 7824-7825.
33. Hillhouse, G. L.; Haymore, B. L. *J. Am. Chem. Soc.* **1982**, *104*, 1537-1548.
34. Mindiola, D. J.; Hillhouse, G. L. *J. Am. Chem. Soc.* **2002**, *124*, 9976-9977.
35. Kaplan, A. W.; Polse, J. L.; Ball, G. E.; Andersen, R. A.; Bergman, R. G. *J. Am. Chem. Soc.* **1998**, *120*, 11649-11662.
36. Polse, J. L.; Andersen, R. A.; Bergman, R. G. *J. Am. Chem. Soc.* **1996**, *118*, 8737-8738.
37. Polse, J. L.; Kaplan, A. W.; Andersen, R. A.; Bergman, R. G. *J. Am. Chem. Soc.* **1998**, *120*, 6316-6328.
38. Albertin, G.; Antoniutti, S.; Bordignon, E.; Carrera, B. *Inorg. Chem.* **2000**, *39*, 4646-4650.
39. Bart, S. C.; Bowman, A. C.; Lobkovsky, E.; Chirik, P. J. *J. Am. Chem. Soc.* **2007**, *129*, 7212-7213.
40. Roland, E.; Walborsky, E. C.; Dewan, J. C.; Schrock, R. R. *J. Am. Chem. Soc.* **1985**, *107*, 5795-5797.
41. Closs, G. L.; Moss, R. A. *J. Am. Chem. Soc.* **1964**, *86*, 4042-4053.
42. Creary, X. *Org. Syn.* **1990**, *7*, 438.
43. Werner, H.; Mahr, N.; Wolf, J.; Fries, A.; Laubender, M.; Bleuel, E.; Garde, R.; Lahuerta, P. *Organomet.* **2003**, *22*, 3566-3576.
44. Mankad, N. P.; Peters, J. C. *Chem. Commun.* **2008**, 1061-1063.

45. Mizobe, Y.; Uchida, Y.; Hidai, M. *Bull. Chem. Soc. Jpn.* **1980**, *53*, 1781-1782.
46. Herrmann, W. A. *Angew. Chem. Int. Ed.* **1978**, *17*, 800-812.
47. Badiel, Y. M.; Warren, T. H. *J. Organomet. Chem* **2005**, *690*, 5989-6000.
48. Dai, X.; Warren, T. H. *J. Am. Chem. Soc.* **2004**, *126*, 10085-10094.
49. Straub, B. F.; Hofmann, P. *Angew. Chem. Int. Ed.* **2001**, *40*, 1288-1290.
50. Waterman, R.; Hillhouse, G. L. *J. Am. Chem. Soc.* **2008**, 12628-12629.
51. Herrmann, W. A.; Hubbard, J. L.; Bernal, I.; Korp, J. D.; Haymore, B. L.; Hillhouse, G. L. *Inorg. Chem.* **1984**, *23*, 2978-2983.
52. Cardin, D. J.; Çetinkaya, B.; Doyle, M. J.; Lappert, M. F. *Chem. Soc. Rev.* **1973**, *2*, 99-144.
53. Mendiratta, A.; Cummins, C. C. *Inorg. Chem.* **2005**, *44*, 7319-7321.
54. Mendiratta, A.; Cummins, C. C.; Kryatova, O. P.; Rybak-Akimova, E. V.; McDonough, J. E.; Hoff, C. D. *Inorg. Chem.* **2003**, *42*, 8621-8623.
55. Tsai, Y.-C.; Stephens, F. H.; Meyer, K.; Mendiratta, A.; Gheorghiu, M. D.; Cummins, C. C. *Organometallics* **2003**, *22*, 2902-2913.
56. Laplaza, C. E.; Odom, A. L.; Davis, W. M.; Cummins, C. C.; Protasiewicz, J. D. *J. Am. Chem. Soc.* **1995**, *117*, 4999-5000.
57. Cherry, J.-P. F.; Johnson, A. R.; Baraldo, L. M.; Tsai, Y.-C.; Cummins, C. C.; Kryatov, S. V.; Rybak-Akimova, E. V.; Capps, K. B.; Hoff, C. D.; Haar, C. M.; Nolan, S. P. *J. Am. Chem. Soc.* **2001**, *123*, 7271-7286.
58. Peters, J. C.; Cherry, J. P. F.; Thomas, J. C.; Baraldo, L.; Mendiola, D. J.; Davis, W. M.; Cummins, C. C. *J. Am. Chem. Soc.* **1999**, *121*, 10053-10067.
59. Smith, M. B.; March, J. *Advanced Organic Chemistry*; Wiley: Hoboken, 2001 p. 1185-1187.
60. Ercolani, C.; Camilli, A.; Sartori, G. *J. Chem. Soc. A* **1966**, 603-605.
61. Kouvetakis, J.; Rittera, C.; Groyb, T. L. *Acta Cryst.* **2000**, e564.
62. Haymore, B. L.; Hughes, M.; Mason, J.; Richards, R. L. *Dalton Trans.* **1988**, 2935 - 2940.
63. Simpson, J. H. *Organic Structure Determination Using 2-D NMR Spectroscopy: A Problem-Based Approach*; Academic Press: Burlington, MA, 2008 p. 110-113.
64. Lowry, T. H.; Richardson, K. S. *Mechanism and Theory in Organic Chemistry*; Harper & Row: New York, 1976 p. 60-71.
65. Jaffe, H. H. *Chem. Rev.* **1953**, *53*, 191-261.
66. Boersch, H. *Monatsch. Chem.* **1934**, *65*, 311-337.
67. Cox, A. P.; Thomas, L. F.; Sheridan, J. *Nature* **1958**, *181*, 1000-1001.
68. Hillhouse, G. L.; Haymore, B. L.; Herrmann, W. A. *Inorg. Chem.* **1979**, *18*, 2423-2426.
69. Head, R. A.; Hitchcock, P. B. *J. Chem. Soc., Dalton Trans.* **1980**, 1150-1155.
70. Seino, H.; Watanabe, D.; Ohnishi, T.; Arita, C.; Mizobe, Y. *Inorg. Chem.* **2007**, *46*, 4784-4786.
71. Chisholm, M. H.; Foltling, K.; Huffinan, J. C.; Ratermann, A. L. *Inorg. Chem.* **1984**, *23*, 2303-2311.
72. Dartiguenave, M.; Joëlle Menu, M.; Deydier, E.; Yves, D.; Siebald, H. *Coord. Chem. Rev.* **1998**, *178-180*, 623-663.
73. Burdett, J. K. *J. Chem. Phys.* **1970**, *52*, 2983-2992.
74. Moore, C. B.; Pimentel, G. C. *J. Chem. Phys.* **1964**, *40*, 342-355.
75. Cowie, M.; Haymore, B. L.; Ibers, J. A. *J. Am. Chem. Soc.* **1976**, *98*, 7608-7617.
76. Haymore, B. L.; Ibers, J. A.; Meek, D. W. *Inorg. Chem.* **1975**, *14*, 541-546.
77. , Due to the strong kinematic coupling between oscillators in [1-H][AlCl₄], the origin of the IR- and Raman-active band found at 1173 cm⁻¹ is uncertain. .
78. Foffani, A.; Pecile, C.; Ghersetti, S. *Tetrahedron* **1960**, *11*, 285-289.
79. Moore, C. B.; Pimentel, G. C. *J. Chem. Phys.* **1964**, *40*, 329-341.
80. Wigley, D. E. *Prog. Inorg. Chem* **1994**, *42*, 239-482.
81. Nugent, W. A.; Mayer, J. M. *Metal-Ligand Multiple Bonds*; Wiley: New York, 1988 p. 33-34.
82. Williams, D. S.; Korolev, A. V. *Inorg. Chem.* **1998**, *37*, 3809-3819.
83. Williams, D. S.; Thompson, D. W.; Korolev, A. V. *J. Am. Chem. Soc.* **1996**, *118*, 6526-6527.
84. Heinselman, K. S.; Hopkins, M. D. *J. Am. Chem. Soc.* **1995**, *117*, 12340-12341.
85. Lakowicz, J. R. *Principles of Fluorescence Spectroscopy*; Springer: New York, 2006 p. 206-207.
86. A Flack x parameter of -0.050(27) was calculated by SHELXL.
87. Müller, P. *Crystal Structure Refinement: A Crystallographer's Guide to SHELXL*; Oxford: New York, 2006 p. 103.
88. Flack, H. D. *Acta Cryst.* **1983**, *A39*, 876-881.
89. Stocker, J. H.; Jenevein, R. M.; Kern, D. H. *J. Org. Chem* **1969**, *34*, 2810-2813.
90. Stocker, J. H.; Jenevein, R. M. *J. Org. Chem* **1968**, *33*, 2145-2146.
91. Dubois, D. L.; Hoffmann, R. *Nouv. J. Chem.* **1977**, *1*, 479-492.
92. Pickett, C. J.; ToIhurst, J. E.; Copenhaver, A.; George, T. A.; Lesterb, R. K. *J. Chem. Soc., Chem. Commun.* **1982**, 1071-1072.
93. Aoshima, T.; Tanase, T.; Mizobe, Y.; Yamamoto, Y.; Hidai, M. *J. Chem. Soc., Chem. Commun.* **1992**, 586-588.
94. Guillemot, G.; Solari, E.; Floriani, C.; Rizzoli, C. *Organomet.* **2001**, *20*, 607-615.
95. Mizobe, Y.; Ono, R.; Uchida, Y.; Hidai, M.; Tezuka, M.; Moue, S.; Tsuchiya, A. *J. Organomet. Chem* **1980**, *204*, 377-385.
96. Savéant, J.-M. *Elements of Molecular and Biomolecular Electrochemistry*; Wiley: Hoboken, 2006 p. 148-150.
97. Mabbott, G. A. *J. Chem. Ed.* **1983**, *60*, 697-702.
98. Olmstead, M. L.; Hamilton, R. G.; Nicholson, R. S. *Anal. Chem.* **1969**, *41*, 260-267.
99. Nicholson, R. S.; Shain, I. *Anal. Chem.* **1964**, *36*, 706-723.
100. McDonough, J. E.; Weir, J. J.; Sukcharoenphon, K.; Hoff, C. D.; Kryatova, O. P.; Rybak-Akimova, E. V.; Scott, B. L.; Kubas, G. J.; Mendiratta, A.; Cummins, C. C. *J. Am. Chem. Soc.* **2006**, *128*, 10295-10303.
101. Savéant, J.-M.; Tessler, D. *J. Phys. Chem* **1978**, *83*, 1723-1727.
102. Constantin, C.; Savéant, J.-M. *J. Electroanal. Chem.* **2004**, *564*, 99-113.
103. Constantin, C.; Savéant, J.-M. *J. Phys. Chem. A* **2005**, *109*, 4125-4132.
104. Savéant, J.-M. *J. Phys. Chem* **1994**, *98*, 3716-3724.
105. Andrieux, C. P.; Grzecczuk, M.; Savéant, J.-M. *J. Am. Chem. Soc.* **1991**, *113*, 8811-8817.
106. Faulkner, L. R.; Bard, A. J. *Electrochemical Methods: Fundamentals and Applications*; Wiley: Hoboken, 2001 p. 512-516.
107. Venkatesan, K.; Blacque, O.; Fox, T.; Alfonso, M.; Schmalle, H. W.; Berke, H. *Organometallics* **2004**, *23*, 1183-1186.
108. Venkatesan, K.; Blacque, O.; Fox, T.; Alfonso, M.; Schmalle, H. W.; Kheradmandan, S.; Berke, H. *Organometallics* **2005**, *24*, 920-932.
109. Venkatesan, K.; Blacque, O.; Berke, H. *Organometallics* **2006**, *25*, 5190-5200.
110. Franceschi, F.; Solari, E.; Floriani, C.; Rosi, M.; Chiesi-Villa, A.; Rizzoli, C. *Chem. Eur. J.* **1999**, *5*, 708-721.
111. THF is coordinated by both Ti and V compounds when n = +2, and for Ti when n = 0.
112. Rosi, M.; Sgamellotti, A.; Franceschi, F.; Floriani, C. *Chem. Eur. J.* **1999**, *5*, 2914-2920.
113. Gallo, E.; Solari, E.; Re, N.; Floriani, C.; Chiesi-Villa, A.; Rizzoli, C. *J. Am. Chem. Soc.* **1997**, *119*, 5144-5154.
114. Shriver, D. F.; Drezdon, M. A. *The Manipulation of Air-Sensitive Compounds*; second ed.; John Wiley & Sons: New York, 1986.
115. Burger, B. J.; Bercaw, J. E. *Experimental Organometallic Chemistry*; Wayda, A. L.; Darensbourg, M. Y., Eds.; American Chemical Society: Washington, DC, 1987, p. 79-98.
116. Pangborn, A. B.; Giardello, M. A.; Grubbs, R. H.; Rosen, R. K.; Timmers, F. J. *Organometallics* **1996**, *15*, 1518-1520.
117. Binsch, G.; Lambert, J. B.; Roberts, B. W.; Roberts, J. D. *J. Am. Chem. Soc.* **1964**, *86*, 5564-70.
118. Sheldrick, G. M. *Acta Cryst.* **1990**, *A46*, 467.
119. Sheldrick, G. M. *SHELXL-97, Program for crystal structure determination*; University of Göttingen; 1997.
120. Sheldrick, G. *Acta Cryst.* **2008**, *A64*, 112-122.
121. te Velde, G.; Bickelhaupt, F. M.; Baerends, E. J.; Fonseca Guerra, C.; van Gisbergen, S. J. A.; Snijders, J. G.; Ziegler, T. *J. Comput. Chem.* **2001**, *22*, 931-967.
122. Fonseca Guerra, C.; Snijders, J. G.; te Velde, G.; Baerends, E. J. *Theor. Chem. Acc.* **1998**, *99*, 391-403.
123. E.J. Baerends, et al. *ADF2004.01*; SCM; 2004.
124. Vosko, S. H.; Wilk, L.; Nusair, M. *Can. J. Phys.* **1980**, *58*, 1200-1211.

125. Becke, A. D. *Phys. Rev. A* **1988**, *38*, 3098-3100.
126. Perdew, J. P. *Phys. Rev. B* **1986**, *34*, 7406.
127. Perdew, J. P. *Phys. Rev. B* **1986**, *34*, 7406-7406.
128. Deng, L. Q.; Schmid, R.; Ziegler, T. *Organometallics* **2000**, *19*, 3069-3076.
129. Lee, C.; Yang, W.; Parr, R. G. *Phys. Rev. B* **1988**, *37*, 785-789.
130. Handy, N. C.; Cohen, A. J. *Mol. Phys.* **2001**, *99*, 403-412.
131. Baker, J.; Pulay, P. *J. Comp. Chem.* **2003**, *24*, 1184-1191.
132. van Lenthe, E.; Baerends, E. J.; Snijders, J. G. *J. Chem. Phys.* **1993**, *99*, 4597-4610.
133. van Lenthe, E.; Snijders, J. G.; Baerends, E. J. *J. Chem. Phys.* **1996**, *105*, 6505-6516.

Table of contents graphic



The preparation of a series of cationic diazoalkane complexes $[4-RC_6H_4C(H)NNMo(N[t-Bu]Ar)_3][AlCl_4]$, $[1-R][AlCl_4]$ ($R = NMe_2, Me, H, Br, CN$, $Ar = 3,5-C_6H_3Me_2$) is described, and the spectroscopic properties of these complexes are compared. One-electron reduction of $[1-R][AlCl_4]$ forms the C–C bonded dimer, $\mu-(4-RC_6H_4C(H)NN)_2[Mo(N[t-Bu]Ar)_3]_2$. The C–C bond in $[1-R]_2$ is redox non-innocent and is broken upon oxidation to regenerate $[1-R]^+$.